Sema3a$_{nestin}^{-/-}$ mice (Fig. 4c and Supplementary Figs 9c, 10, 11a), and both CGRP- and TRPV1-postive fibres were also neurofilament positive (Supplementary Fig. 11b). In addition, the innervation of these fibres into cortical bone was also reduced (Supplementary Fig. 11c), demonstrating that the projections of peripheral nerve fibres into bone tissue are uniformly decreased, in agreement with all of the bones being affected in *Sema3a*$_{synapsin}^{-/-}$ and *Sema3a*$_{nestin}^{-/-}$ mice. To examine rigorously disturbances in nerve innervation in *Sema3a*$_{synapsin}^{-/-}$ and *Sema3a*$_{nestin}^{-/-}$ mice, we performed three different experiments. First, *Sema3a*$_{synapsin}^{-/-}$ and *Sema3a*$_{nestin}^{-/-}$ mice were intercrossed with *Sox10*-Venus mice, which express Venus fluorescent protein under the control of a *Sox10* promoter[24]. Venus-positive sensory nerve innervation was significantly decreased in *Sema3a*$_{synapsin}^{-/-}$ and *Sema3a*$_{nestin}^{-/-}$ mice (Supplementary Fig. 12). Second, the retrograde fluorescent tracer, Fluoro-Gold, was injected into the bone marrow of *Sema3a*$_{synapsin}^{-/-}$ and *Sema3a*$_{nestin}^{-/-}$ mice, resulting in fewer neurons being labelled in the DRG (Supplementary Fig. 13). Last, sensory evaluation revealed that *Sema3a*$_{synapsin}^{-/-}$ and *Sema3a*$_{nestin}^{-/-}$ mice were anaesthetic to all of the tested stimuli, indicating functional sensory deficits in these mice (Supplementary Fig. 14). Taken together, these results demonstrated the disruption of nerve innervation in *Sema3a*$_{synapsin}^{-/-}$ and *Sema3a*$_{nestin}^{-/-}$ mice. Importantly, a longitudinal analysis showed that bone mass and nerve innervation into bone were decreased at all analysed time points in *Sema3a*$_{synapsin}^{-/-}$ and *Sema3a*$_{nestin}^{-/-}$ mice (that is, from embryo to 3 months old; Figs 3b–d, 4a, c and Supplementary Figs 6a, b, 7b–d, f–h, 15), which further indicated that bone mass accrual during development required normal nerve innervation into bone.

We also confirmed that the projections of CGRP-positive sensory fibres into bone were similarly decreased in *Sema3a*$^{-/-}$ mice (Fig. 4c), whereas DBH-positive sympathetic nerve fibres were unaffected (Fig. 4b). By contrast, the projections of peripheral nerve fibres into bone tissues were not affected in *Sema3a*$_{col1}^{-/-}$, *Sema3a*$_{osx}^{-/-}$ or *Sema3a*$^{+/-}$ mice (Supplementary Fig. 16), which had normal bone mass, indicating that the abnormal projections of sensory fibres, not the expression of Sema3A in bone, are responsible for the bone abnormalities in *Sema3a*$^{-/-}$, *Sema3a*$_{synapsin}^{-/-}$ and *Sema3a*$_{nestin}^{-/-}$ mice.

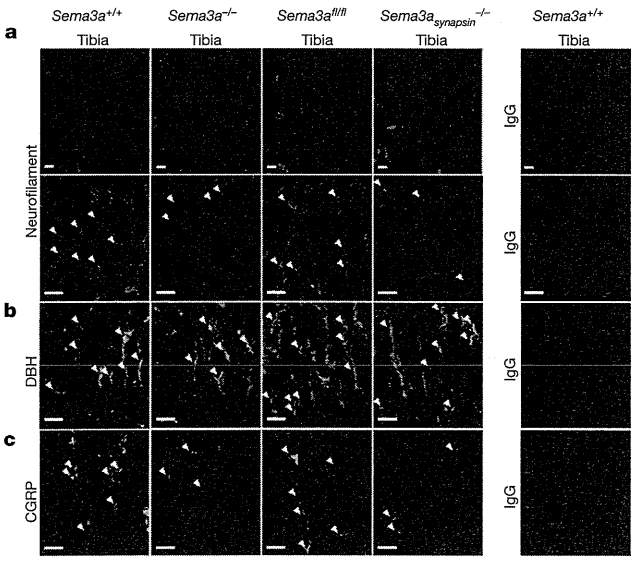

Figure 4 | Neuron-derived Sema3A is indispensable for sensory nerve innervation into bone. **a–c**, Longitudinal section of tibiae from *Sema3a*$^{-/-}$, *Sema3a*$_{synapsin}^{-/-}$ and control mice at postnatal day 3 ($n = 3$), immunostained for neurofilament (**a**, red), DBH (**b**, green) or CGRP (**c**, green) fibres (arrowheads). Representative pictures are shown from at least three separate experiments. Note a decrease of nerve innervation in *Sema3a*$^{-/-}$ or *Sema3a*$_{synapsin}^{-/-}$ mice (**a**, **c**). Scale bars, 100 μm.

To address formally the causal relationship between abnormal sensory development and low bone mass, we intercrossed Sema3A-floxed mice with nestin-CreERT mice[25] expressing a tamoxifen-inducible Cre recombinase under the control of a nestin promoter, and injected tamoxifen after birth to bypass the effect of Sema3A on sensory nervous system development (*Sema3a*$_{nestin}^{ERT-/-}$ mice). Tamoxifen treatment did not significantly affect nerve innervation or bone mass accrual in *Sema3a*$_{nestin}^{ERT-/-}$ mice, which indicated that Sema3A expression during development before birth is essential for nerve innervation (Supplementary Fig. 17)—a prerequisite for normal bone mass accrual. Second, wild-type mice treated with capsaicin lost bone mass and showed decreased sensory innervation[26] (Supplementary Fig. 18). However, *Sema3a*$_{nestin}^{-/-}$ mice, which had diminished bone mass and sensory innervation in the absence of capsaicin treatment (Supplementary Figs 7b–d, f–h, 9, 11a), did not exhibit a further loss in bone mass with capsaicin treatment (Supplementary Fig. 18). Collectively, these results suggested that abnormal development of the sensory nervous system or disruption of the capsaicin-sensitive TRPV1-positive sensory nerves led to low bone mass. Moreover, *Sema3a*$_{synapsin}^{-/-}$ and *Sema3a*$_{nestin}^{-/-}$ mice also showed reduced bone regeneration and defective nerve innervation into newly synthesized bone after femoral bone marrow ablation (Supplementary Fig. 19), indicating that Sema3A also participated in bone modelling in adult mice via the modulation of nerve innervation.

To investigate the role of the Sema3A signalling pathway in nerve innervation in bone, we analysed *Plxna4*$^{-/-}$ mice[27]. *Plxna4*$^{-/-}$ mice developed a low bone mass phenotype and showed decreased nerve innervation in bone (Supplementary Fig. 20), reminiscent of the *Sema3a*$_{synapsin}^{-/-}$ and *Sema3a*$_{nestin}^{-/-}$ mice phenotypes. These results suggested that the Sema3A–Plxna4 pathway is important for nerve innervation in bone.

We next determined whether other neuronal abnormalities in *Sema3a*$^{-/-}$ mice were also observed in *Sema3a*$_{synapsin}^{-/-}$ mice. The abnormal development of the olfactory system and spinal cord[6], reduced thickness of the cerebral cortex[6], and altered pattern of sympathetic innervation in the heart[28] that are characteristics of *Sema3a*$^{-/-}$ mice were identified in *Sema3a*$_{synapsin}^{-/-}$ mice (Supplementary Fig. 21). These results suggested that, *in vivo*, neuron-derived Sema3A contributes to normal nervous system development; that is, Sema3A works as an autocrine factor for neuronal development.

We demonstrate that neuron-derived Sema3A regulates bone remodelling through the modulation of sensory nerve projections into bone. A potential direct action of Sema3A on osteoblasts has been suggested recently using global Sema3A knockout mice and a supraphysiological dose of Sema3A (ref. 13). However, given the absence of bone abnormalities in *Sema3a*$_{col1}^{-/-}$ and *Sema3a*$_{osx}^{-/-}$ mice, Sema3A must physiologically regulate bone metabolism primarily through the modulation of sensory nerve innervation, *in vivo*, although this does not rule out the possibility that osteoblast-derived Sema3A has a role in bone metabolism[13].

Although Sema3A has strong inhibitory effects on axonal elongation *in vitro* when added exogenously[23], we demonstrated that Sema3A, which is produced in neurons, is indispensable in the normal development of peripheral neurons *in vivo*. The co-expression of Npn1 and Sema3A in motor neurons regulates axon sensitivity to environmental Sema3A sources during motor axon pathfinding[29]. Given that Sema3A is expressed in DRG sensory nerves (Supplementary Fig. 22) and that *Sema3a*$_{synapsin}^{-/-}$ mice exhibit phenotypic similarities with *Sema3a*$^{-/-}$ mice (Supplementary Fig. 21), Sema3A expression in neurons may be a fundamental component of proper neural development.

This is, to our knowledge, the first study to demonstrate that sensory nerves have an essential role in bone remodelling. The sympathetic nervous system is known to inhibit bone mass accrual, yet a 'sensing' system is required to achieve bone homeostasis. Therefore, an intriguing question is whether any interaction exists between 'osteo-anabolic' afferent sensory nerves and 'osteo-catabolic' efferent sympathetic nerves.

Clinically, familial dysautonomia patients, who are characterized by the loss of unmyelinated axons including sensory nerves, suffer from osteoporosis[30], supporting the importance of sensory nerves in bone homeostasis. Further studies are necessary to determine whether other bone degenerative diseases, including osteoporosis, involve a loss of sensory nervous system integrity.

METHODS SUMMARY

To delete Sema3A in osteoblasts and neurons, we mated Sema3A-floxed mice[7] with α1(I)-Cre[17] mice or osx-Cre[18] mice, or synapsin-I-Cre[20] mice or nestin-Cre[21] mice. Histomorphometry and microcomputed tomography analysis were performed as previously described. Primary osteoblasts and osteoclasts were cultured as previously described. Fluorescent immunohistochemistry was performed as previously described. Detailed experimental information is described in Methods.

Full Methods and any associated references are available in the online version of the paper.

Received 16 February 2012; accepted 21 March 2013.
Published online 5 May 2013.

1. Kruger, R. P., Aurandt, J. & Guan, K. L. Semaphorins command cells to move. *Nature Rev. Mol. Cell Biol.* **6,** 789–800 (2005).
2. Tamagnone, L. & Comoglio, P. M. To move or not to move? Semaphorin signalling in cell migration. *EMBO Rep.* **5,** 356–361 (2004).
3. Pasterkamp, R. J. & Giger, R. J. Semaphorin function in neural plasticity and disease. *Curr. Opin. Neurobiol.* **19,** 263–274 (2009).
4. Tran, T. S., Kolodkin, A. L. & Bharadwaj, R. Semaphorin regulation of cellular morphology. *Annu. Rev. Cell Dev. Biol.* **23,** 263–292 (2007).
5. Roth, L. *et al.* The many faces of semaphorins: from development to pathology. *Cell. Mol. Life Sci.* **66,** 649–666 (2009).
6. Behar, O., Golden, J. A., Mashimo, H., Schoen, F. J. & Fishman, M. C. Semaphorin III is needed for normal patterning and growth of nerves, bones and heart. *Nature* **383,** 525–528 (1996).
7. Taniguchi, M. *et al.* Disruption of semaphorin III/D gene causes severe abnormality in peripheral nerve projection. *Neuron* **19,** 519–530 (1997).
8. Nakamura, F. *et al.* Increased proximal bifurcation of CA1 pyramidal apical dendrites in *sema3A* mutant mice. *J. Comp. Neurol.* **516,** 360–375 (2009).
9. Tian, L., Rauvala, H. & Gahmberg, C. G. Neuronal regulation of immune responses in the central nervous system. *Trends Immunol.* **30,** 91–99 (2009).
10. Potiron, V., Nasarre, P., Roche, J., Healy, C. & Boumsell, L. Semaphorin signaling in the immune system. *Adv. Exp. Med. Biol.* **600,** 132–144 (2007).
11. Adams, R. H. & Eichmann, A. Axon guidance molecules in vascular patterning. *Cold Spring Harb. Perspect. Biol.* **2,** a001875 (2010).
12. Neufeld, G. & Kessler, O. The semaphorins: versatile regulators of tumour progression and tumour angiogenesis. *Nature Rev. Cancer* **8,** 632–645 (2008).
13. Hayashi, M. *et al.* Osteoprotection by semaphorin 3A. *Nature* **485,** 69–74 (2012).
14. Negishi-Koga, T. *et al.* Suppression of bone formation by osteoclastic expression of semaphorin 4D. *Nature Med.* **17,** 1473–1480 (2011).
15. Takegahara, N. *et al.* Plexin-A1 and its interaction with DAP12 in immune responses and bone homeostasis. *Nature Cell Biol.* **8,** 615–622 (2006).
16. Hall, A. & Lalli, G. Rho and Ras GTPases in axon growth, guidance, and branching. *Cold Spring Harb. Perspect. Biol.* **2,** a001818 (2010).
17. Dacquin, R., Starbuck, M., Schinke, T. & Karsenty, G. Mouse α1(I)-collagen promoter is the best known promoter to drive efficient Cre recombinase expression in osteoblast. *Dev. Dyn.* **224,** 245–251 (2002).
18. Rodda, S. J. & McMahon, A. P. Distinct roles for Hedgehog and canonical Wnt signaling in specification, differentiation and maintenance of osteoblast progenitors. *Development* **133,** 3231–3244 (2006).
19. Takeda, S. Central control of bone remodelling. *J. Neuroendocrinol.* **20,** 802–807 (2008).
20. Zhu, Y. *et al.* Ablation of NF1 function in neurons induces abnormal development of cerebral cortex and reactive gliosis in the brain. *Genes Dev.* **15,** 859–876 (2001).
21. Okada, S. *et al.* Conditional ablation of Stat3 or Socs3 discloses a dual role for reactive astrocytes after spinal cord injury. *Nature Med.* **12,** 829–834 (2006).
22. Méndez-Ferrer, S. *et al.* Mesenchymal and haematopoietic stem cells form a unique bone marrow niche. *Nature* **466,** 829–834 (2010).
23. Mach, D. B. *et al.* Origins of skeletal pain: sensory and sympathetic innervation of the mouse femur. *Neuroscience* **113,** 155–166 (2002).
24. Shibata, S. *et al. Sox10*-Venus mice: a new tool for real-time labeling of neural crest lineage cells and oligodendrocytes. *Mol. Brain* **3,** 31 (2010).
25. Imayoshi, I., Ohtsuka, T., Metzger, D., Chambon, P. & Kageyama, R. Temporal regulation of Cre recombinase activity in neural stem cells. *Genesis* **44,** 233–238 (2006).
26. Offley, S. C. *et al.* Capsaicin-sensitive sensory neurons contribute to the maintenance of trabecular bone integrity. *J. Bone Miner. Res.* **20,** 257–267 (2005).
27. Suto, F. *et al.* Plexin-A4 mediates axon-repulsive activities of both secreted and transmembrane semaphorins and plays roles in nerve fiber guidance. *J. Neurosci.* **25,** 3628–3637 (2005).
28. Ieda, M. *et al.* Sema3a maintains normal heart rhythm through sympathetic innervation patterning. *Nature Med.* **13,** 604–612 (2007).
29. Moret, F., Renaudot, C., Bozon, M. & Castellani, V. Semaphorin and neuropilin co-expression in motoneurons sets axon sensitivity to environmental semaphorin sources during motor axon pathfinding. *Development* **134,** 4491–4501 (2007).
30. Maayan, C., Bar-On, E., Foldes, A. J., Gesundheit, B. & Pollak, R. D. Bone mineral density and metabolism in familial dysautonomia. *Osteoporos. Int.* **13,** 429–433 (2002).

Supplementary Information is available in the online version of the paper.

Acknowledgements We thank M. Taniguchi and G. Karsenty for discussions; F. Suto and H. Fujisawa for *Plxna4*$^{-/-}$ mice; M. Ukegawa, H. Inose, M. Iwata, S. Ohba, T. Hara and G. Itai for technical assistance. This work was supported by the Funding Program for Next Generation World-Leading Researchers (NEXT Program) to S.T., a grant-in-aid for scientific research from the Japan Society for the Promotion of Science to S.T. and T.F., and grants from the National Institute of Neurological Disorders and Stroke (NS065048) to Y.Y.

Author Contributions T.F. conducted most of the experiments. R.X., H. Ochi, A.K., Z.G., Y.Y., C.M., C.X., T.H., Y.A. and M.E. conducted mice analyses. T.S., K.F., W.B. and S. Sunamura conducted *in vitro* experiments. S. Shibata and H. Okano generated mutant mice. A.O., H.I. and K.S. discussed the project. S.T. wrote most of the manuscript. S.T. designed and supervised the project.

Author Information Reprints and permissions information is available at www.nature.com/reprints. The authors declare no competing financial interests. Readers are welcome to comment on the online version of the paper. Correspondence and requests for materials should be addressed to S.T. (shu-tky@umin.ac.jp).

METHODS

Animals. Sema3A-knockout mice (RBRC01104) and floxed Sema3A mice (RBRC01106) were provided by RIKEN BRC. Transgenic mice expressing Cre recombinase under the control of the α1(I)-collagen promoter (col1-Cre)[17], osterix promoter (osx-Cre)[18], synapsin I promoter (synapsin-I-Cre)[20] and nestin promoter (nestin-Cre)[21], were mated with floxed mice to obtain conditional knockout mice. nestin-CreERT mice were described previously[25]. For neonatal activation of CreERT, 83.5 mg kg^{-1} tamoxifen (Sigma) in corn oil (Sigma) was intraperitoneally injected into lactating mothers once a day for five consecutive days from the day of delivery. For histological experiments, corn-oil-treated mice were used as controls. At 8 weeks, mice were subjected to histological experiments. For capsaicin treatment, mice were deprived of drinking water for 6 h before capsaicin injection to prevent pulmonary oedema. Capsaicin (Sigma) and vehicle (10:10:80 (v/v) of Tween-80, ethanol, saline) were freshly prepared each time, capsaicin was sonicated in vehicle until homogenously suspended, and mice were injected subcutaneously above the dorsal spine. Four-week-old mice received two rounds of capsaicin or vehicle treatment. In each round, mice received daily injections for three consecutive days (10 mg kg^{-1} on days 1 and 2, and 15 mg kg^{-1} on day 3), and each round was seven days apart. At 8 weeks, mice were subjected to histological experiments. To obtain *Sema3a*$_{nestin}^{-/-}$;*Sox10*-Venus transgenic mice, *Sema3a*$_{nestin}^{f/+}$;*Sox10*-Venus mice[24] were mated with *Sema3a*$^{f/f}$ mice. *Plxna4*$^{-/-}$ mice were previously described[28].

We maintained all the mice under a 12 h light–dark cycle with *ad libitum* access to regular food and water, unless specified. All animal experiments were performed with the approval of the Animal Study Committee of Keio university school of medicine and conformed to relevant guidelines and laws.

Cell culture. *In vitro* primary osteoblast cultures were established as previously described[31,32]. Briefly, calvarial osteoblast cells were isolated from 4-day-old mice by enzymatic digestion in α-minimal essential medium (α-MEM) with 0.5 mg ml^{-1} collagenase-P (Roche) and 0.05% trypsin. For osteoblastic differentiation, cells (3×10^4 cells per cm^2) were cultured in osteogenic medium (0.1 mg ml^{-1} ascorbic acid, 10 mM β-glycerophosphate). Medium was changed every 2 days. After 7 days, osteoblastic differentiation was confirmed by the measurement of ALP activity and expression of osteoblastic marker genes. Results are representative of more than four individual experiments. The murine preosteoblast cell line MC3T3-E1 was cultured in α-MEM. Cells were seeded (3×10^4 cells per cm^2) and treated with osteogenic medium with or without recombinant mouse Sema3A Fc chimaera (R&D systems). Medium was changed every 2 days. After 7 days, ALP measurement was performed. Results are representative of more than four individual experiments. *In vitro* osteoclast differentiation was accomplished as previously described[33]. Briefly, bone marrow cells (3×10^5 cells per cm^2) of 6- to 8-week-old mouse femurs were cultured in α-MEM supplemented with FBS in the presence of human macrophage colony-stimulating factor (M-CSF, 10 ng ml^{-1}; R&D Systems) for 2 days and then differentiated into osteoclasts using human RANKL (50 ng ml^{-1}; Peprotech) and M-CSF for 3 days. Subsequently, the differentiation of osteoclasts was evaluated by TRAP staining. Results are representative of more than four individual experiments. The proliferation assay for osteoblasts was performed using the Cell Counting kit-8 (DOJINDO), according to the manufacturer's instructions. Results are representative of more than four individual experiments.

Transfection and infection. For the Sema3A knockdown study, MC3T3-E1 cells were seeded (3×10^4 cells per cm^2) and transfected with 20 nM of short interfering (si)Sema3A (Invtrogen) or siControl (Invtrogen) using HiPerFect (Qiagen) according to the manufacturer's instructions. siRNA sequences were 5′-AAUAGUUGUUG GUUCCCGGAAGACG-3′ and 5′-CGUCUUCCGGGAACCAACAACUAUU-3′ (for *Sema3a*). After transfection, cells were cultured with osteoblastic differentiation media. Culture medium was changed every 2 days. Recombinant mouse Sema3A Fc chimaera (R&D systems) was added every 2 days at indicated concentrations. After 7 days, osteoblastic differentiation was confirmed by the measurement of ALP activity. Results are representative of more than four individual experiments. To confirm Sema3A intracellular signalling, MC3T3-E1 cells (3×10^4 cells per cm^2) were infected with adenovirus containing a dominant-negative form of Rac1 (T17N) or enhanced green fluorescent protein (eGFP). Infected cell were cultured in osteogenic medium with or without Sema3A (2 μg ml^{-1}). Medium was changed every 2 days. After 7 days, ALP measurement was performed. Results are representative of more than four individual experiments.

Histological and histomorphometric analyses. We injected mice with calcein (25 mg kg^{-1}; Sigma) and stained undecalcified sections of the lumbar vertebrae using von Kossa and TRAP as previously described[34]. We performed static and dynamic histomorphometric analyses using the Osteomeasure Analysis System (Osteometrics) following nomenclature defined by the American Society for Bone and Mineral research as previously described[34]. Bone volume/tissue volume (BV/TV; %), bone formation rate/bone surface (BFR/BS; μm^3 μm^{-1} yr^{-1}), mineral apposition rate (MAR; mm yr^{-1}) osteoblast surface/bone surface (Ob. S/BS; %) and osteoclast number/bone perimeter (No. Oc./B. Pm) were analysed. Oc. S/BS and No. Oc./B. Pm were calculated on TRAP staining slices.

Micro-CT analyses. We obtained two-dimensional images of the distal femurs by micro-CT analysis (μCT; Comscan).

Measurement of deoxypyridinoline cross-links. We measured serum deoxypyridinoline cross-links (DPD) with the MicroVue tDPD kit (QUIDEL) according to the manufacturer's instructions.

Quantitative real-time PCR analysis. Total RNA from tissues and cultured cells was extracted using TRizol reagent (Invitrogen) and reverse transcription was performed by ReverTra Ace qPCR RT Kit (TOYOBO) according to the manufacturer's instructions. We performed quantitative analysis of gene expression using the Mx3000P real-time PCR system (Agilent Technologies). We used *Gapdh* expression as an internal control. The following primers were used: *Sema3a* sense, 5′-TGGGC TGGTTCACTGGGATTGC-3′ and *Sema3a* antisense, 5′-CTGGAGCTGTTGG CCAAGCCAT-3′; *Alpl* sense, 5′-ACACCTTGACTGTGGTTACTGCTGA-3′ and *Alpl* antisense, 5′-CCTTGTAGCCAGGCCCGTTA-3′; *Bglap* sense, 5′-TCTGAC AAAGCCTTCATGTCCA-3′ and *Bglap* antisense, 5′-CGGTCTTCAAGCCATA CTGGTC-3′; *Dmp1* sense, 5′-CCCAGAGGGACAGGCAAATA-3′ and *Dmp1* antisense, 5′-TCCTCCCCACTGTCCTTCTT-3′; *Plxna1* sense, 5′-GAGTGCAA GGAAGCTTTTGC-3′ and *Plxna1* antisense, 5′- TCCTCAATCCCAGGAAACAG-3′; *Plxna2* sense, 5′- GGGGGCTATCAATCGTGTCT-3′ and *Plxna2* antisense, 5′- AGGG CTGTACAATGAGGGGT-3′; *Plxna3* sense, 5′- GCCAACCCACCTCGGCAGAC-3′ and *Plxna3* antisense, 5′- GCAGAGGGGTGTTGATGCAGGG-3′; *Plxna4* sense, 5′- A TCTAGAGTGGCGACAAGGAAG-3′ and *Plxna4* antisense, 5′- TGGAGACAGTGG AGTTGTTCAC-3′; *Nrp1* sense, 5′- GAAGCACCGAGAAAACAAGG-3′ and *Nrp1* antisense, 5′- TTGCCTTCGAACGACTTAGC-3′; *Gapdh* sense, 5′-ACCCAGAAGAC TGTGGATGG-3′ and *Gapdh* antisense, 5′-CACATTGGGGGTAGGAACAC-3′.

Immunohistochemistry. Bones were directly embedded into OCT after dissection. Brains and spinal cords were fixed in 4% paraformaldehyde (PFA) in 0.1 M phosphate buffered saline (PBS) for 24 h and dehydrated in 30% sucrose in 0.1 M PBS for 48 h. Brain, lumbar spinal cord and olfactory bulbs were dissected and embedded in 1.5% low-melting-temperature agarose (BM Equipment) in PBS. Brains were cut into 25-μm-thick coronal sections using a cryostat and slices from every 150 μm were used. Lumbar spinal cords were cut into 25-μm-thick axial sections. To characterize the expression of neuronal markers in the brain, series of sections from each experimental group were stained with neuronal markers. After treatment with 0.2% Triton X-100 for 5 min, sections were blocked with 5% NGS and incubated with monoclonal antibodies, SMI31 (a marker for neurofilament M+H, 1:500, COVANCE), polyclonal antibodies, CGRP (1:800, BioMol), TRPV1 (1:300, Transgenic), tyrosine hydroxylase (TH) (1:500 Chemicon), DBH (1:500 Chemicon) for 24 h as previously described[35]. Primary antibodies were visualized with goat anti-mouse IgG Alexa-594 (1:500, Molecular Probes) and goat anti-rabbit IgG Alexa-488 (1:400, Molecular Probes).

For quantification of innervations of nerve fibres, the percentage of neurofilament-positive (red) area to the area corresponding to the secondary spongiosa of the right proximal tibial metaphyses was calculated by Image J software (http://rsbweb.nih.gov/ij/).

Retrograde labelling of tibia afferents. To assess tibia afferents, retrograde tracing with Fluoro-Gold (FG: Fluorochrome) was performed in wild-type and *Sema3a*$_{nestin}^{-/-}$ mice. A total of 2 μl of 4% FG was injected into the right tibial tuberosity with a Hamilton syringe. The DRGs were transcardially perfused with a solution of 4% PFA in PBS 1 week after the FG injection and carefully dissected. The L3 and L4 DRGs were cut into 10-μm-thick transverse sections perpendicular to the spinal nerve using a cryostat. The sections were incubated with NeuroTrace green fluorescent Nissl stain (Invitrogen). The numbers of FG-positive neurons were counted in the section of middle portion of DRG.

Sensory behavioural tests. The mice were placed in plexiglass boxes, which were 9.5 × 21 × 25 cm in size, to become acclimated to the testing environment. These boxes were then placed on an elevated perforated plastic surface for a minimum of 30 min before all behavioural tests. A blind observer conducted the behavioural testing.

In the tactile threshold test, mechanical sensitivity was measured by applying a series of calibrated von Frey filaments (0.02–8 g) to the plantar aspect of the hind paw. Each filament was applied once to each mouse. Beginning with the 1 g filament, each filament was applied perpendicular to the hind paw for 4–6 s. A brisk withdrawal of the hind paw indicated a positive response, and a lack of withdrawal indicated a negative response. This filament testing is repeated a maximum of two additional times, and a 2/3 response to the filament indicated an overall positive response. If the mouse demonstrated an overall positive response, the next lower force filament was applied as described above. In case an overall positive response was not observed (0/3 or 1/3 responses), the next greater force filament was applied as described above. Once the crossover threshold could be determined (that is,

from response to no response, or vice versa), the responses to the next five filaments were recorded to determine the median withdrawal threshold.

Response to acetone was tested using a plastic tube connected to a 1 ml syringe and 100 µl of acetone was applied to the plantar surface of the foot without touching the skin. Acetone was applied five times to each paw at an interval of at least 30 s, and the number of brisk foot withdrawals in response to the acetone application was recorded.

Response to noxious heat stimulus was tested in the following manner. A response latency to a noxious heat source was measured with a hot plate apparatus (NISSIN, Japan). Mice were placed on a surface heated to 50 or 55 °C, and the amount of time between placement on the apparatus and a hindpaw lick or jump was recorded. To avoid tissue damage due to prolonged exposure to the heated surface, we used a cut-off time of 45 s.

Bone marrow ablation. Mice were anaesthetized intraperitoneally with 400 mg kg^{-1} trichloroacetaldehyde monohydrate (Chloral Hydrate; Wako Pure Chemical). After removal of the hair from both hind limbs, the bone marrow of both femora on each animal was ablated as described previously[36]. Briefly, bilateral longitudinal incisions were made on the knees of each mouse to expose the femoral condyle by dislocation of the patella. A hole was made at the intercondylar notch of the femur using a dental drill. A 0.6 mm diameter Kirschner wire was inserted in the proximal end of the femur to confirm completion of marrow ablation by radiography. After removal of the Kirschner wire, the dislocated patella was reposed and the skin was sutured. Mice were killed at day 7 after ablation and bone histological analyses were performed.

***In situ* hybridization.** Spinal cords were fixed in 4% PFA in PBS and dehydrated in 30% sucrose in PBS. Frozen sections (20 µm) were hybridized with digoxigenin (DIG)-labelled antisense riboprobes corresponding to a partial cDNA of mouse *Sema3a* (3,852–4,378 bp) at 60 °C overnight. For detection, signals were developed using anti-digoxigenin antibody conjugated with alkaline phosphatase. After antibody treatment, sections were incubated with NBT/BCIP (Roche).

Statistical analysis. We performed statistical analysis using Tukey–Kramer and Student's *t*-test. Values were considered statistically significant at $P < 0.05$. All data are represented as mean ± s.d. Results are representative of more than four individual experiments.

31. Kimura, A. *et al.* Runx1 and Runx2 cooperate during sternal morphogenesis. *Development* **137,** 1159–1167 (2010).
32. Inose, H. *et al.* A microRNA regulatory mechanism of osteoblast differentiation. *Proc. Natl Acad. Sci. USA* **106,** 20794–20799 (2009).
33. Fujita, K. *et al.* Vitamin E decreases bone mass by stimulating osteoclast fusion. *Nature Med.* **18,** 589–594 (2012).
34. Sato, S. *et al.* Central control of bone remodeling by neuromedin U. *Nature Med.* **13,** 1234–1240 (2007).
35. Kusano, K. *et al.* Enhancement of sciatic nerve regeneration by adenovirus-mediated expression of dominant negative RhoA and Rac1. *Neurosci. Lett.* **492,** 64–69 (2011).
36. Okuda, N. *et al.* ED-71, a novel vitamin D analog, promotes bone formation and angiogenesis and inhibits bone resorption after bone marrow ablation. *Bone* **40,** 281–292 (2007).

CORRECTIONS & AMENDMENTS

CORRIGENDUM

doi:10.1038/nature12418

Corrigendum: Sema3A regulates bone-mass accrual through sensory innervations

Toru Fukuda, Shu Takeda, Ren Xu, Hiroki Ochi, Satoko Sunamura, Tsuyoshi Sato, Shinsuke Shibata, Yutaka Yoshida, Zirong Gu, Ayako Kimura, Chengshan Ma, Cheng Xu, Waka Bando, Koji Fujita, Kenichi Shinomiya, Takashi Hirai, Yoshinori Asou, Mitsuhiro Enomoto, Hideyuki Okano, Atsushi Okawa & Hiroshi Itoh

Nature **497**, 490–493 (2013); doi:10.1038/nature12115

In this Letter the left panels of Fig. 2a show images of a femur from a semaphorin 3A-knockout ($Sema3a_{col1}^{-/-}$) mouse, rather than from a littermate $Sema3a^{f/f}$ mouse. Figure 1 shows the correct panels. This error does not affect our conclusions and the legend of Fig. 2 is correct.

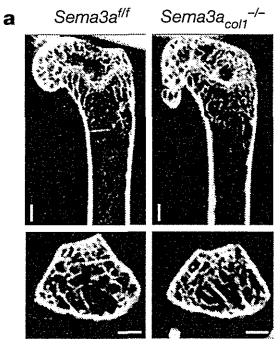

Figure 1 | This figure shows the microcomputed tomography panels of Fig. 2a with the left panels corrected.

nature COMMUNICATIONS

ARTICLE

Received 24 Apr 2013 | Accepted 10 Oct 2013 | Published 12 Nov 2013

DOI: 10.1038/ncomms3740 OPEN

Chondroitin sulphate *N*-acetylgalactosaminyl-transferase-1 inhibits recovery from neural injury

Kosei Takeuchi[1,2], Nozomu Yoshioka[1,2,3,4], Susumu Higa Onaga[1], Yumi Watanabe[1,2,4], Shinji Miyata[5], Yoshino Wada[1], Chika Kudo[1], Masayasu Okada[1,6], Kentaro Ohko[1,7], Kanako Oda[8], Toshiya Sato[8], Minesuke Yokoyama[8], Natsuki Matsushita[9], Masaya Nakamura[10], Hideyuki Okano[11], Kenji Sakimura[12], Hitoshi Kawano[3], Hiroshi Kitagawa[5] & Michihiro Igarashi[1,2]

Extracellular factors that inhibit axon growth and intrinsic factors that promote it affect neural regeneration. Therapies targeting any single gene have not yet simultaneously optimized both types of factors. Chondroitin sulphate (CS), a glycosaminoglycan, is the most abundant extracellular inhibitor of axon growth. Here we show that mice carrying a gene knockout for CS *N*-acetylgalactosaminyltransferase-1 (T1), a key enzyme in CS biosynthesis, recover more completely from spinal cord injury than wild-type mice and even chondroitinase ABC-treated mice. Notably, synthesis of heparan sulphate (HS), a glycosaminoglycan promoting axonal growth, is also upregulated in TI knockout mice because HS-synthesis enzymes are induced in the mutant neurons. Moreover, chondroitinase ABC treatment never induces HS upregulation. Taken together, our results indicate that regulation of a single gene, *T1*, mediates excellent recovery from spinal cord injury by optimizing counteracting effectors of axon regeneration—an extracellular inhibitor of CS and intrinsic promoters, namely, HS-synthesis enzymes.

[1] Department of Neurochemistry and Molecular Cell Biology, Brain Research Institute, Niigata University, 1-757 Asahi-machi, Niigata 951 8510, Japan. [2] Center for Transdisciplinary Research, Brain Research Institute, Niigata University, 1-757 Asahi-machi, Niigata 951 8510, Japan. [3] Laboratory of Neural Regeneration, Tokyo Metropolitan Institute of Medical Science, 2-1-6 Kamikitazawa, Tokyo 156 8506, Japan. [4] Doctoral and restart postdoctoral fellowship program, Japan Society for the Promotion of Science (JSPS), Tokyo 102 8472, Japan. [5] Department of Biochemistry, Kobe Pharmaceutical University, 4-19-1 Motoyamakita-machi, Kobe 658 8558, Japan. [6] Department of Neurosurgery, Brain Research Institute, Niigata University, 1-757 Asahi-machi, Niigata 951 8510, Japan. [7] Department of Dermatology, Graduate School of Medical and Dental Sciences, Brain Research Institute, Niigata University, 1-757 Asahi-machi, Niigata 951 8510, Japan. [8] Department of Comparative and Experimental Medicine, Brain Research Institute, Niigata University, 1-757 Asahi-machi, Niigata 951 8510, Japan. [9] Translational Research Center (TRC), Ehime University Hospital, Shitsukawa, Ehime 791-0295, Japan. [10] Department of Orthopedics, Keio University School of Medicine, 35 Shinanomachi, Tokyo 160 8582, Japan. [11] Departments of Physiology, Keio University School of Medicine, 35 Shinanomachi, Tokyo 160 8582, Japan. [12] Department of Cellular Neurobiology, Brain Research Institute, Niigata University, 1-757 Asahi-machi, Niigata 951 8510, Japan. Correspondence and requests for materials should be addressed to M.I. (email: tarokaja@med.niigata-u.ac.jp).

Many patients with spinal cord injury (SCI) suffer from severe paralysis[1,2], possibly because injured axons in the adult mammalian central nervous system (CNS), including those in humans, rarely regenerate[1,2]. Recent findings demonstrate that the regulation of both extracellular and intrinsic factors that affect axon regeneration is essential to recovery from adult CNS neuronal injury[3,4]. Reduction or overexpression of intracellular cell-autonomous regulators promotes axon regrowth[5–11]; however, controlled manipulation of the endogenous expression of these molecules is challenging[8]. Regrettably, current protocols for removing or reducing the extracellular inhibitors do not result in axon regeneration sufficient for complete recovery from SCI.

Chondroitin sulphate (CS), a glycosaminoglycan (GAG) produced mainly by reactive astrocytes and partly by NG2 proteoglycan-positive cells after SCI, is the most widely distributed and most potent inhibitor of axon regeneration[3,5–7,12]. CS degradation resulting from application of chondroitinase ABC (ChABC), a bacterial enzyme, to the injury site promotes some additional axon regeneration[6]. Many practical methods can effectively provide ChABC near injury sites; notably, methods involving viral vector delivery of *ChABC*[13–15] result in more axon sprouting[16] (see reviews[17,18]). In addition, we must consider treatment alternatives; specifically, we must recognize that CS may be physiologically necessary to minimize the inflammation and limit its area after SCI by inhibiting invasion of macrophages[19,20]. Thus, complete removal of CS may exacerbate, not ameliorate, SCI.

Here we focused on optimizing CS synthesis following SCI. The process of the CS synthesis is very complicated, and more than 10 enzymes participate in CS synthesis[21–23] (Fig. 1a). Notably, heparan sulphate (HS) is also a GAG and a potent promoter of axonal growth, and the first enzymatic step of CS synthesis and of HS synthesis are the same[24]. Therefore, the second step in CS synthesis, catalysed by CS *N*-acetylgalactosaminyltransferase-1 (abbreviated as T1 in this paper), is the first unique and rate-limiting step in CS synthesis; consequently, T1 is tightly regulated because it begins CS-specific polysaccharide chain synthesis[24–28].

Here we generated T1-knockout (T1KO) mice[29] and induced SCI in these and wild-type (WT) mice to investigate the mechanism of recovery from compression-induced (70 kdyne impact force) SCI. T1KO mice exhibited significantly better recovery from SCI based on locomotor behaviours and histological analysis than did untreated WT or ChABC-treated WT mice. Synthesis of HS, as also upregulated in T1KO mice because expression of HS-synthesis enzymes was induced. Notably, ChABC treatment never induced

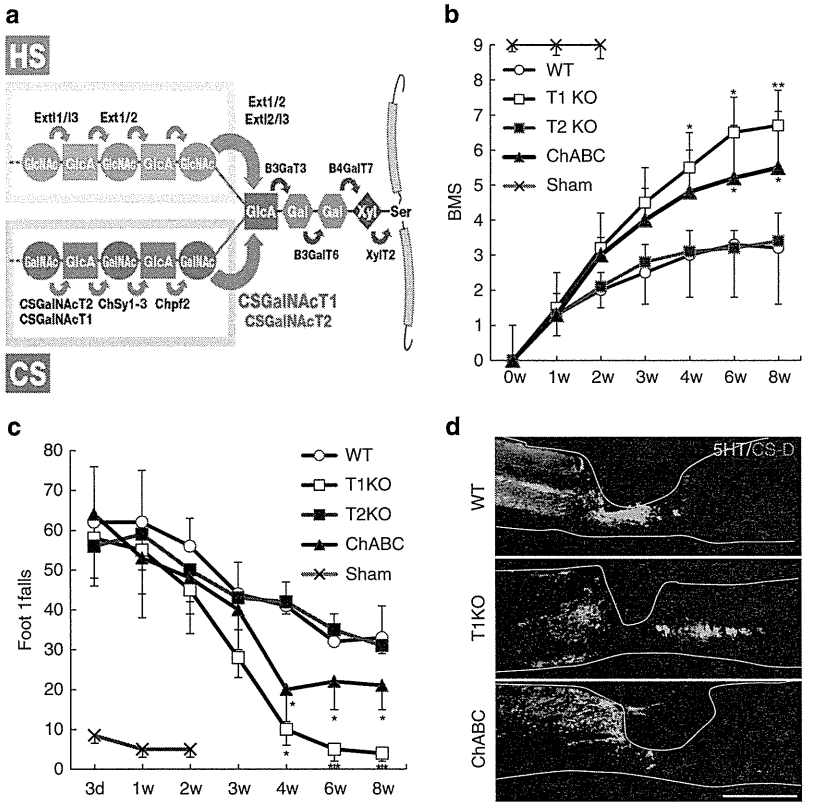

Figure 1 | T1KO mice recover from SCI more quickly and more completely than WT mice. (**a**) Schematic diagram of GAG synthesis. The steps in CS synthesis are as follows: (1) synthesis of the tetrasaccharide linker that is attached to core proteins; (2) attachment of an *N*-acetylgalactosamine (GalNAc) to the linker; (3) addition of glucuronic acid (GlcA) to GalNAc and subsequent polymerization of the disaccharide backbone (GalNAc-GlcA); and (4) sulphation of several sites (**a**). During CS or HS synthesis T1 transfers GalNAc (CS) to the linker, whereas Ext1/Ext2 transfers GlcNAc (HS). T1 is primarily responsible for the catalysis of the first unique step in CS chain formation[21,22,26,28] (**a**); therefore, T1 is the most important enzyme for regulation of CS synthesis. See Supplementary Table S2 for a description of enzyme abbreviations. Gal, galactose; GalNAc, *N*-acetylgalactosamine; GlcNAc, *N*-acetylglucosamine; GlcA, glucuronic acid; Xyl, xylose. (**b**) BMS scores after SCI. (**c**) Footfall tests after SCI. (**b**,**c**) T1KO versus WT and ChABC. *Post hoc* analyses were conducted using the Bonferroni–Dunn test for repeated-measures ANOVA. In **b** and **c**, data are expressed as the mean ± s.e.m; $^{*}P<0.05$; $^{**}P<0.01$ ($n=9$; ANOVA). (**d**) Immunohistochemistry of 5HT(+) axon terminals in mice 8 weeks after SCI. 5HT (green) and CS (red). Scale bars, 1 mm.

HS upregulation. Judging from our results and those from two previous reports, an HS-synthesizing enzyme Ext2 satisfies the definition of a potential intrinsic growth regulator in neurons[30,31]. Our results indicate that a single gene, that encodes T1, is a promising therapeutic target for SCI treatment.

Results

T1KO recover more rapidly than WT and ChABC-treated mice. We had focused on optimizing CS synthesis following SCI. However, the formation of a tetrasaccharide linker is notably the first step in both CS and HS biosynthesis, and CS inhibits axonal regrowth, whereas HS promotes it (Fig. 1a). Therefore, the second step in CS and HS synthesis—which is catalysed by T1 and the Ext1-Ext2 heterodimer (Ext1/Ex2), respectively—is the first unique and rate-limiting step in each pathway. These enzymes share a substrate, the tetrasaccharide linker[21], and they bifurcate GAG synthesis into two alternative pathways[24,26]. Although CS *N*-acetylgalactosaminyltransferase-2 (CSGalNAcT2; abbreviated as T2 in this paper) is a T1 isoform, it has lower enzyme activity than does T1[21,27].

We focused on reducing T1 activity, via gene knockout, as a potential treatment for SCI. T1KO mice are viable, but they have abnormal bone development and 10% shorter bodies than do WT mice[29] (see Supplementary Fig. S1a–c). Following induced SCI, we examined and compared the recoveries of T1KO, T2-knockout (T2KO), untreated WT and ChABC-treated WT mice. Recovery of motor functions following SCI was evaluated using the Basso mouse scale (BMS) scoring[32] (Fig. 1b), footfall tests (Fig. 1c; Supplementary Movie 1), footprint analysis (Supplementary Fig. S2a,b) and electromyography (Supplementary Fig. S2c); T1KO mice recovered from SCI more quickly and more completely than did T2KO, ChABC-treated WT or untreated WT mice (Fig. 1b,c; also see Supplementary Fig. S2d,e). The areas encompassing serotonin-positive (5HT(+)) terminals[1] beyond the lesion site were much larger in T1KO than in untreated WT or ChABC-treated WT mice (Fig. 1d, Table 1 and Supplementary Fig. S2f,g), and there were many more 5HT(+) terminals in T1KO mice (Table 1; see also Supplementary Fig. S2f,g). These observations indicated that functional recovery after SCI was associated with axon regrowth and/or sprouting (Fig. 1d and Table 1) in T1KO mice. Importantly, these effects in T1KO mice were superior to those following ChABC treatment (Table 1 and Supplementary Fig. S2g), and T2KO mice did not show any significant increase in 5HT(+) staining (Fig. 1e and Supplementary Fig. S2f,g). To determine whether the corticospinal tract (CST; a representative pathway operating voluntary movement) recovered, we traced the biotinylated dextran amine (BDA) (+)-extending axons in each group of mice after SCI. Axons that had migrated past a scar (Supplementary Fig. S3a,b) and into caudal regions were evident only in T1KO SCI mice (Supplementary Fig. S3b). GAP-43 immunoreactivity—which is a marker of neuron growth, growth cones and extending axons[14,33]—was evident in CST axons in caudal regions only in T1KO SCI mice, but not in ChABC-treated WT or T2KO SCI mice (Supplementary Fig. S3c). Following SCI, caudal GAP-43(+)-CST axon terminals were significantly more abundant in T1KO SCI mice than in WT or T2KO mice (Supplementary Fig. S3d,e).

Next, we examined whether the superior recovery and axon regrowth in T1KO animals depended on reduction of CS. We used immunohistochemistry to confirm that ChABC treatment broke CS down (Supplementary Fig. S4a). T1 was highly expressed in some reactive astrocytes in WT mice following SCI, but it was not evident in T1KO mice (Supplementary Fig. S4b). Moreover, CS production in areas with glial scars, which are produced by reactive astrocytes[3], was much lower in T1KO mice than WT or T2KO mice (Fig. 2a). We also demonstrated biochemically (Fig. 2b) and using morphometrical measurements (Fig. 2c) that CS levels in injured spinal cords of T1KO mice were lower than in those of WT or T2KO mice (Supplementary Fig. S4c). Undoubtedly, several other enzymes are involved in CS synthesis[28] (*cf.* Fig. 1a), and CS is not completely absent from T1KO mice[29] (Fig. 2c; Supplementary Fig. S4d). Notably, *Caenorhabditis elegans* lacks T1 and T2, yet a chondroitin backbone comprising GalNAc and GlcA is synthesized in worms by four other enzymes (ChSy1–3 and Chpf2) that are also found in mammals[34] (see Fig. 1a); therefore, these four enzymes may synthesize CS in mammals lacking T1, although probably at a much slower rate than when T1 is present.

Table 1 | Quantification of areas encompassing 5HT(+) terminals.

	2~3 mm rostral	Lesion	2~3 mm caudal	4~5 mm caudal
WT	8,780 ± 1,345	926 ± 21	85 ± 10	30 ± 11
T1KO	8,942 ± 1,137	365 ± 32	2,779 ± 897*	2,025 ± 910*
T2KO	8,765 ± 1,029	902 ± 41	72 ± 12	26 ± 13
ChABC	6,238 ± 3,547	643 ± 92	779 ± 615*	1,151 ± 505*

ChABC, ChABC-treated; Sham, Sham-operated.
The areas encompassing 5HT(+) terminals in the ventral horn were measured 6 weeks after injury[32] (see also Supplementary Fig. S2e). Data are expressed as the mean ± s.e.m. ANOVA and Bonferroni's multiple comparison test (Prism 5.04); $n = 9$;
*$P < 0.05$ (versus WT).

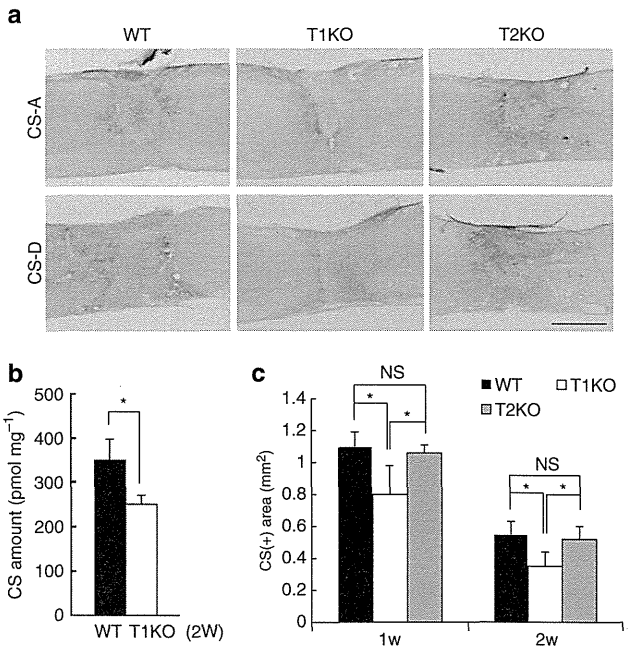

Figure 2 | CS synthesis after the CSI is lower in T1KO than in WT mice. (**a**) Following SCI, CS expression 2 weeks after the injury was considerably lower in T1KO mice than in WT or T2KO mice. Anti-CS-A and anti-CS-D antibodies recognize two distinct sugar chain units of CS. Scale bar, 1 mm. (**b**) CS accumulation following SCI was lower in T1KO than in WT mice. *$P < 0.05$ (Student's *t*-test; $n = 5$). (**c**) CS(+) areas were smaller in T1KO (grey) mice than in WT (white) or T2KO (grey) mice. Repeated-measures ANOVA followed by the Bonferroni–Dunn test. *$P < 0.05$ ($n = 6$). Data are expressed as the mean ± s.e.m. in **b** and **c**.

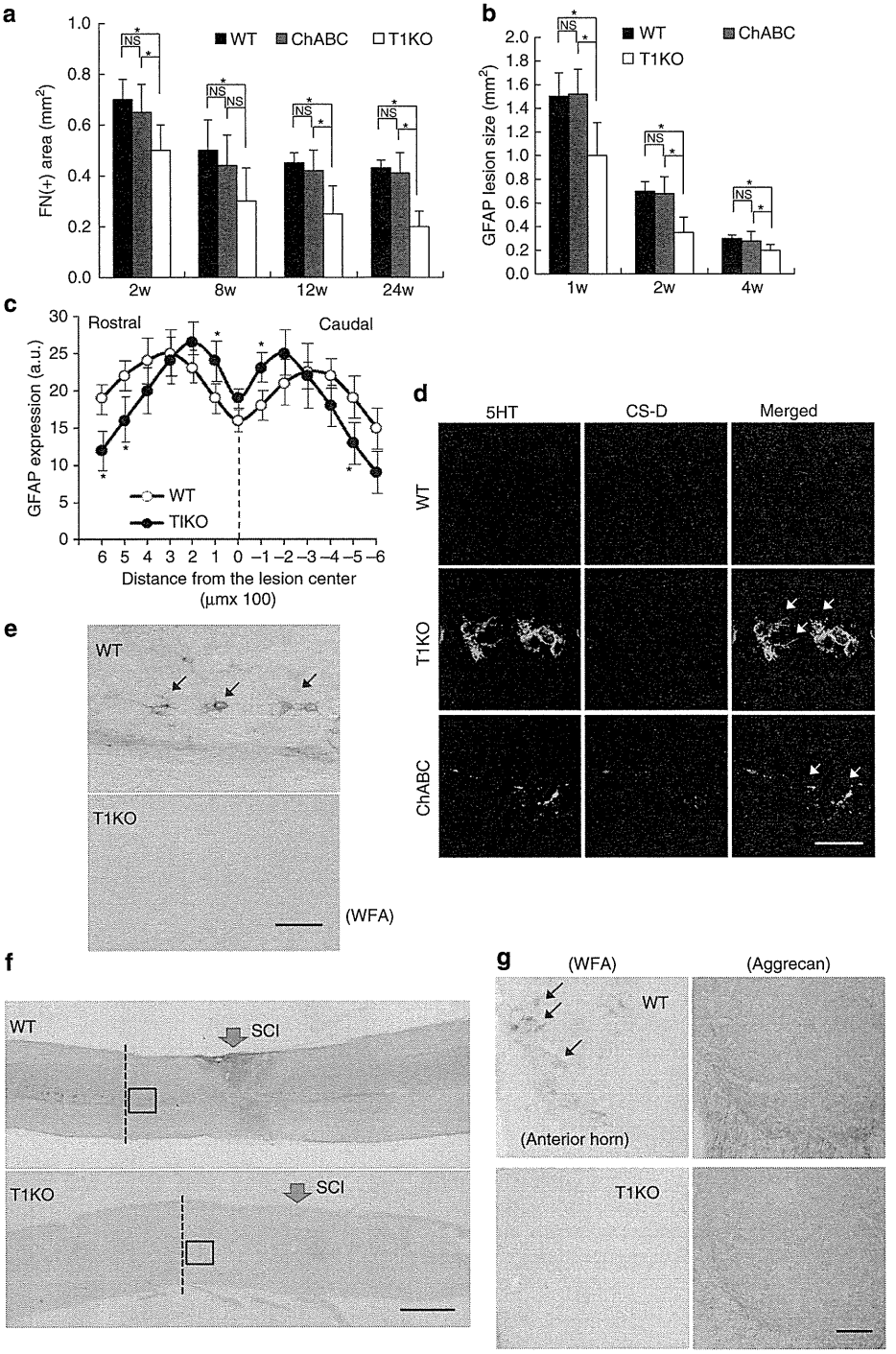

Figure 3 | Reduced CS levels are associated with reduced scar formation in T1KO mice. In **a** and **b**, $n=7$; and in **c**, $n=5$. (**a**,**b**) Fibrotic scar areas (**a**) and glial scar areas (**b**) were smaller in T1KO mice (grey) than in WT (white) or in ChABC-treated mice (ChABC; black). Data are expressed as the mean ± s.e.m. These data were compared by two-way ANOVA and Bonferroni's *post hoc* pairwise comparisons; $^*P<0.05$. (**c**) Glial scars in T1KO mice covered a narrow area that surrounded the lesion centre; these areas were narrower than those in WT mice (2 weeks after SCI). Data are expressed as the mean ± s.e.m. Scheffe's *post hoc* tests at each spinal segment showed significant differences between T1KO and WT mice at −5, −1 (caudal) and 1, 5, 6 (rostral) mm away from the lesion epicentre ($^*P<0.05$). (**d**) Distribution of 5HT(+) terminals after recovery from SCI in T1KO mice was different from that in ChABC-treated (ChABC) mice. Many sprouting 5HT(+) terminals had accumulated in extracellular matrix around the cells in T1KO, but not in ChABC-treated mice. Arrows indicate the regrowing 5HT(+) terminals. Scale bar, 50 μm. (**e**–**g**) PNNs after SCI were not evident in T1KO mice. Higher (**e**) and lower (**f**) magnifications of WFA-labelled PNNs in WT and in T1KO 3 weeks after SCI. PNNs were evident in WT but not in T1KO mice. The boxed areas in **f** are magnified in **e**. Scale bars, 1 mm (**e**,**f**). (**g**) Coronal sections of the anterior horn were taken along the axis represented by the dotted line in **f** and stained via WFA or with anti-aggrecan antibody (aggrecan). In T1KO mice, WFA-labelled CS concentrated in PNN was not evident but signal from aggrecan, a core CSPG protein, was evident. Scale bars, 50 μm.

Nevertheless, fibrotic scars (Fig. 3a) and glial scars[3,19–20] (Fig. 3b) were much smaller in T1KO mice than in WT or ChABC-treated mice (Fig. 3a,b; Supplementary Fig S3a). In contrast, scar area did not differ significantly between ChABC-treated and WT mice (Fig. 3a,b). Each glial scar in T1KO mice was limited to a narrow area that surrounded the centre of the SCI lesion (Fig. 3c; Supplementary Fig. S3a). 5HT(+) terminals in T1KO mice were highly concentrated around the astrocytes but scars in ChABC-treated mice were not (Fig. 3d). These results indicated that both effects of T1KO—more complete axon regrowth and more regrowing axon terminals (Fig. 1b–d, and Table 1)—were related to a reduction in the 'barrier' scar area and that this reduction was a result of decreased CS production[3,6,7] (Figs 2 and 3). Moreover, each effect was probably independent of residual CS in T1KO mice because ChABC treatment caused more CS degradation and led to worse outcomes than did T1KO (Fig. 3a,b and Table 1). ChABC treatment reportedly reduces the perineuronal net (PNN), which is enriched with CS and inhibits neural plasticity[35]; moreover, reductions in the PNN reportedly enhance neuronal plasticity, neuronal sprouting and recovery from SCI[36,37]. Therefore, we examined the PNN in mice recovering from induced SCI. We used *Wisteria floribunda* agglutinin (WFA), a generalized marker of PNN, to assess PNNs and found that WFA was evident in WT mice but not in T1KO mice (Fig. 3e–g).

Increased HS synthesis in T1KO mice promotes rapid recovery. On the basis of histological and phenotypic features of T1KO mice, we doubted that the 25% reduction in CS (Fig. 2c) in T1KO mice was solely responsible for such complete recovery from SCI (Fig. 1b–d, Table 1 and Supplementary Fig. S2a,b,d,e,g). Therefore, we suspected that changes in HS synthesis might also be involved because T1 and some HS-synthesis enzymes share the tetrasaccharide linker as a substrate[24,28] (Fig. 1a). The expression of enzymes other than T1 that synthesize CS in response to SCI was not significantly different between injured T1KO and injured WT mice (Supplementary Fig. S5a). Surprisingly, however, the expression of HS-synthesis enzymes—including Ext1 and Ext2, which are essential to HS synthesis (Fig. 1a)—was much higher in injured T1KO mice than that in uninjured T1KO or injured WT mice (Fig. 4a). Importantly, ChABC treatment did not cause upregulation of these HS-synthesis enzymes (Supplementary Fig. S6a).

On the basis of these results, we strongly suspected that HS synthesis contributed to the superior recovery of T1KO mice; therefore, we examined HS expression after SCI. HS-positive areas were significantly larger in the injured spinal cords of T1KO mice than in those of WT mice (Fig. 4b), and HS levels were 20-fold higher in the injured regions of T1KO mice than in those of WT (Fig. 4c; Supplementary Fig. S6b). Notably, neither ChABC treatment nor T2 knockout increased HS levels (Fig. 4b,d; Supplementary Fig. S6c). There were no significant differences between injured T1KO and injured WT mice in the expression of any CS-containing proteoglycan (CSPG) or syndecan-3, which is an HS-containing proteoglycan (HSPG; Supplementary

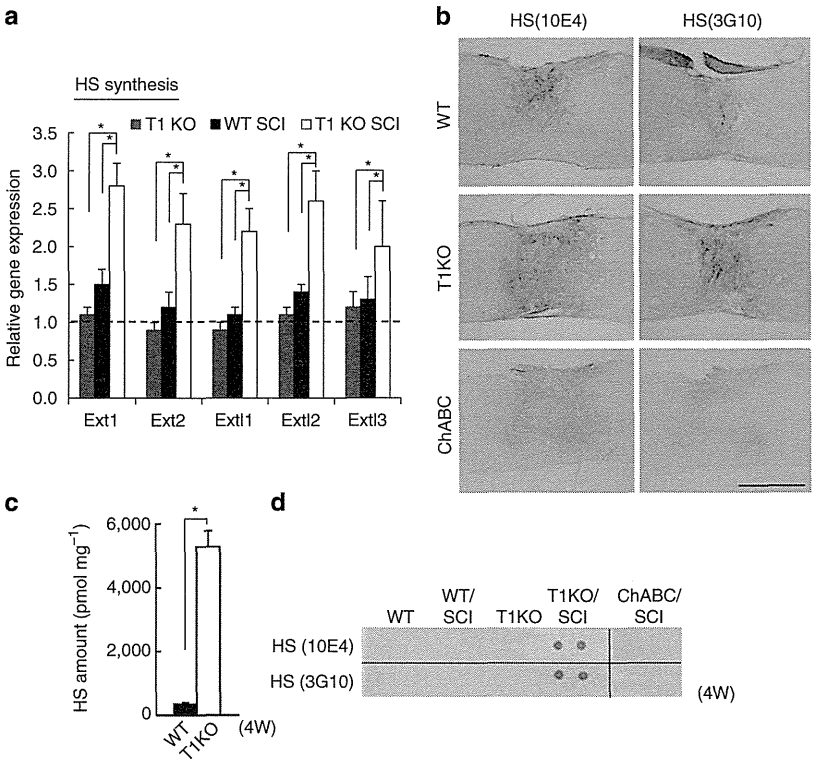

Figure 4 | HS synthesis increases in injured spinal cords of T1KO mice. T1KO, T1-null; WT, wild type. Data are expressed as the mean ± s.e.m. (**a,c**). (**a**) Expression of messenger RNAs encoding enzymes necessary for HS synthesis was assayed via reverse transcriptase-PCR. The level of mRNA expression in WT mice was defined as 1.0 for each gene. These data were compared by two-way ANOVA and Bonferroni's *post hoc* pairwise comparisons. $^*P<0.05$ ($n=15$); T1KO SCI versus WT SCI or versus T1KO (intact). (**b**) On the basis of immunohistochemistry, HS was highly expressed in T1KO mice but not in WT or ChABC-treated mice, 2 w after SCI. Antibodies 10E4 and 3G10 recognize different disaccharides in HS. Scale bar, 1 mm. (**c**) Biochemical quantification of HS expression at sites of SCI 2 weeks after injury. $^*P<0.05$ (Student's *t*-test; $n=6$). (**d**) Dot-blot analysis of HS expression in spinal cords before and after SCI (2 w). HS was detected only in T1KO mice with SCI, but not in any other mice, including the ChABC-treated mice.

Fig. S6a,d). To assess whether this upregulation of HS synthesis in T1KO mice following SCI promoted axon regrowth or sprouting, we examined the effects of continuously administered bacterial heparitinase (HSase), which degrades HS[30], on recovery from SCI. On the basis of BMS scoring (Fig. 5a) and footfall tests (Fig. 5b), HSase treatment slowed the recovery of T1KO mice (Fig. 5 and Table 2), as did RNA interference (RNAi)-mediated knockdown (KD) of an HS-synthesis enzyme, Ext1 (Fig. 5 and Table 2). In addition, HSase treatment reduced the area encompassing regenerating 5HT(+) axon terminals in T1KO mice to a level similar to that in WT mice (Table 2), but the recovery in ChABC-treated mice was not sensitive to HSase, suggesting that ChABC did not induce HS upregulation (Supplementary Fig. S6a,e). These results indicated that upregulation of HS synthesis in T1KO mice promoted axon regrowth and/or sprouting and functional recovery from SCI, just as it promotes axon growth during CNS development[5,25].

We tried to identify the target HSPGs in injured T1KO mice that bore the upregulated HSase-sensitive HS. HS-modified syndecan-3 (*N*-syndecan) and glypican-1 were highly expressed (Fig. 6a and Supplementary Fig. S6d) and widely distributed (Fig. 6b) at sites of SCI in T1KO mice. In the injured spinal cords of T1KO mice, both HSPGs were detected via HS-specific antibodies (Fig. 6c) and had HSase-sensitive HS chains (Fig. 6d); importantly, in WT SCI mice, degraded HS derived from these two HSPGs was barely evident, indicating that the upregulated HSase-sensitive HS was specifically bound to syndecan-3 and glypican-1 in injured T1KO (Fig. 6d).

After SCI, Ext2 was expressed in neurons[30] of T1KO mice (Fig. 7a), and the expression of HS-synthesis enzymes was upregulated in neuron-rich areas rather than in areas of glial scarring (Fig. 7b); therefore, we concluded that extra HS was produced by the neurons[5,24,25] that expressed HS-synthesis enzymes such as Ext2. Receptor protein tyrosine phosphatase-σ (RPTPσ), a receptor for both HSPGs and CSPGs[38,39], was also upregulated in T1KO mice after SCI, and RPTPσ co-localized with some of the regrowing and/or sprouting axons (Supplementary Fig. S7a–d). HS, unlike CS, is known to promote axon growth during neural development[5,24,25,31,39]; therefore, our data indicated that GAG synthesis in T1KO mice was more favourable to axon regrowth than was the GAG synthesis in WT mice. To assess whether upregulation of HS was directly involved in neurite growth following SCI and whether effects of RPTPσ on neurite growth depended on HS, we examined the effects of concurrent overexpression of Ext1 and Ext2 on cultured neurons (Fig. 7c). Ext1-Ext2 overexpression induced neurite growth in an HSase-sensitive (Fig. 7c) and RPTPσ-sensitive (Supplementary Fig. S7e) manner[39], indicating that upregulation of HS contributed to axon growth. Therefore, HS-synthesis enzymes such as Ext2 may promote axon growth intrinsically in neurons by targeting new HS synthesis to syndecan-3, glypican-1 or both[40]. *RPTPσ* messenger RNA expression and RPTPσ levels were elevated in WT, ChABC-treated and T1KO mice (Supplementary Fig. S7c,d), indicating that at least the increased axon regrowth was not due to a RPTPσ-dependent reduction in CS.

RNAi-mediated T1 KD (T1-KD) *in vivo* led to excellent recovery from SCI (Supplementary Fig. S8a–e). T1-KD-associated scars were similar in size to T1KO-associated scars (Supplementary Fig. S8f). T1-KD caused reduced CS synthesis (Supplementary Fig. S8g), and scar sizes were significantly smaller following T1-KD than following ChABC treatment (Supplementary Fig. S8h). Moreover, downregulation of CS synthesis and upregulation of HS-synthesis enzymes were induced by simultaneous T1-KD and T2-KD, as well as by T1KO (Supplementary Fig. S9a–c and Fig. 4, also see

Table 2 | Quantitative analysis of the area of the caudal region covered by 5HT(+) terminals after HSase treatment 4 weeks after injury.

	2~3 mm rostral	Lesion	2~3 mm caudal	4~5 mm caudal
WT + PBS	8,501 ± 1,522	799 ± 31	81 ± 11	32 ± 14
T1KO + PBS	8,862 ± 1,204	415 ± 51	2,398 ± 991*	2,012 ± 813*
T1KO + HSase	5,703 ± 3,134	512 ± 107	719 ± 337*	698 ± 173*
ChABC + HSase	6,021 ± 3,467	740 ± 153	800 ± 593*	1,003 ± 566*

ChABC, ChABC-treated; HSase, HSase-treated.
These data were compared by two-way ANOVA and Bonferroni's multiple comparison test (Prism 5.04). T1KO + PBS versus T1KO + HSase, WT + PBS or ChABC + HSase.
*$P<0.05$ ($n=5$)

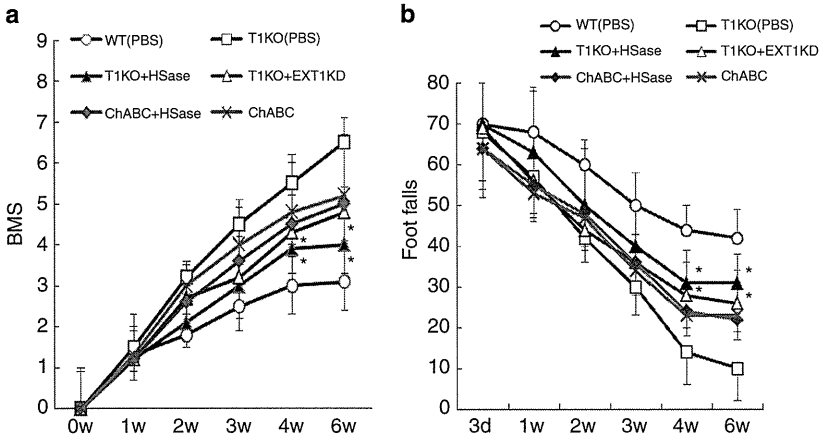

Figure 5 | Increased HS promotes more rapid and more complete recovery from SCI. T1KO, T1-null; WT, wild type. Data are expressed as the mean ± s.e.m. (**a**) BMS scores and (**b**) footfall tests with or without reduction of HS in WT, T1KO and ChABC-treated mice; ChABC was used at 0.2 U per 00 μl. HSase (0.4U per 200 μl; experimental treatment) or PBS (control treatment) was administered via a minipump. *EXT1KD*; KD of Ext1 by *in vivo* RNAi (100 nmol per 200 μl); also see Supplementary Fig. S8a. *Post hoc* analyses were conducted using the Bonferroni–Dunn test for repeated-measures ANOVA. *$P<0.05$ ($n=5$; in **a** and **b**). The BMS subscore for T1KO versus T1KO + HSase mice or versus T1KO + EXT1 KD were significantly different at 4 and 6 weeks after SCI.

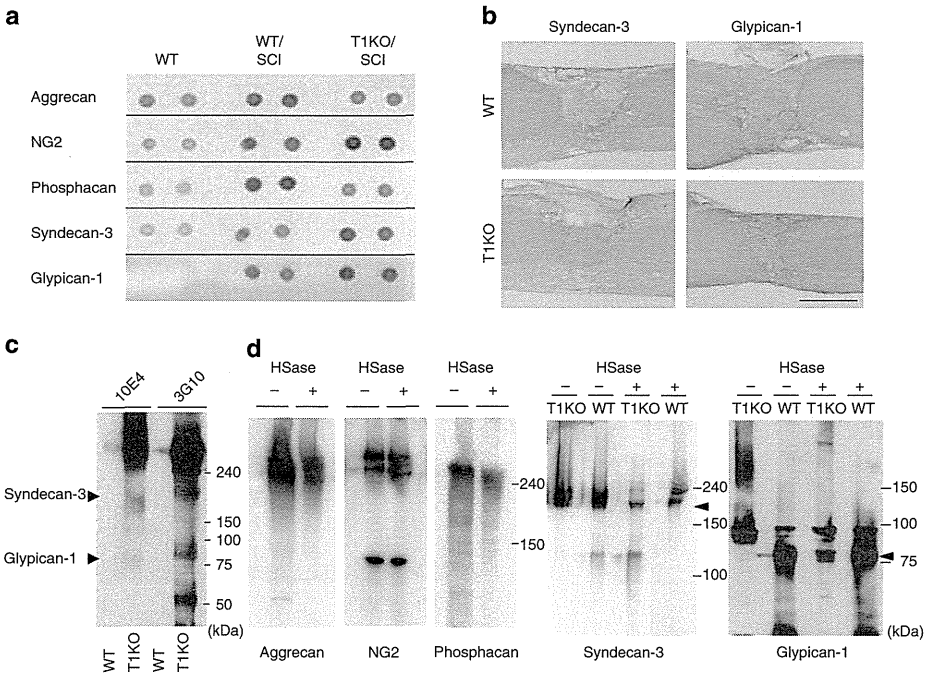

Figure 6 | Syndecan-3 and glypican-1 are the target HSPGs of SCI-induced HS upregulation in T1KO mice. (**a**,**b**) Syndecan-3 and glypican-1, HSPGs derived from neurons, were expressed in T1KO mice after SCI (2 weeks). (**a**) Dot-blot analysis of the major core proteins decorated with CSPG or HSPG. (**b**) Immunohistochemistry of syndecan-3 and glypican-1 after SCI (2 weeks) in WT and in T1KO mice. Scale bar, 1 mm. (**c**) HSase-treated HSPGs detected by 3G10, the antibody that recognized the HS stub. At least three distinct HSPGs were recognized by 3G10 in T1KO SCI mice, but not in WT SCI mice, including 180 kDa (syndecan-3) and 65–80 kDa (glypican-1). (**d**) Western-blot analysis of PGs near the lesion sites before (−) and after (+) HSase treatment (5 mU; 37 °C, 3 h). Notably, syndecan-3 and glypican-1 were the main PGs with HSase-sensitive HS in injured T1KO mice. The data for CSPG core proteins (aggrecan, NG2 or phosphacan) are shown only for the injured T1KO mice, and each CSPG was HSase insensitive. Arrows indicate the position of deglycosylated proteins. Numbers on the right indicate molecular masses (kDa).

Supplementary Fig. S5a,b); notably, T1-KD alone was insufficient to cause both effects (Supplementary Fig. S9c,d; compared with Supplementary Fig. S9a,b).

Discussion

T1KO mice had significantly better recovery from SCI than did WT or ChABC-treated mice (Fig. 1b–d); three distinct phenomena were responsible for this superior recovery. First, T1KO reduced CS synthesis and resulted in smaller scars than did ChABC treatment; reduced scaring probably contributed to better recovery because the smaller scars introduced smaller physical and weaker chemical barriers to the regrowing or the sprouting axons (Figs 1e, 2c and 3a–d, and Supplementary Fig. S2f). In addition, T1KO probably reduced CS concentrations (Fig. 3e). Notably, reduction of CS was apparently superior to complete elimination of CS for SCI recovery, probably because CS has some positive roles in recovery (Fig. 8a). Second, simultaneous upregulation of HS synthesis and downregulation of CS in T1KO mice were essential to excellent recovery from SCI. HS promotes axon growth[5,24,25], and syndecan-3, a target HSPG of SCI-induced HS upregulation, is enriched in axons and the extracellular matrix around axons[41]. T1KO and T1-KD + T2-KD (Supplementary Fig. S9c) produced the most favourable environment for recovery from SCI; specifically, these treatments shifted conditions at the injury away from the non-permissive CS-rich state (Fig. 8a,b). It is evident that T1KO was substantially superior to ChABC treatment specifically because HS synthesis was stimulated by T1KO and never by ChABC treatment (Fig. 5a,b, Table 2 and Supplementary Fig. S5a,d). HSPGs are important for signal transduction, axon growth and axon guidance[24,42]; therefore, our findings are very important to axon regeneration. Third, expression of HS chains on both syndecan-3 and glypican-1 and expression of HS-synthesis enzymes (for example, Ext2, Ext1 and Extl2) in neurons were essential to the superior recovery from SCI of T1KO mice (Figs 4a,d, 6a,c and 7a,b). Taken together, our results and those from two previous reports indicated that Ext2 satisfies the definition of a potential intrinsic growth regulator in neurons; the most relevant findings are that Ext1/2 expression is developmentally downregulated in the CNS[43] and that Ext2 and syndecan-1 expressions in neurons are specifically upregulated during peripheral nerve regeneration[30]. Lack of T1 evidently induced these intrinsic positive regulators of axon growth[4,10]. These HS-synthesis enzymes belong to a newly identified group of 'development-dependent factors with axon growth-promoting features' and are totally different from previously described factors such as PTEN and KLFs[9,11]. Therefore, we conclude that T1KO and ChABC treatment led to recovery from SCI by very distinct mechanisms.

The following two strategies for controlling CS synthesis have been developed: first, a deoxyribozyme targeting *Xylt1* (see Fig. 1a) messenger RNA inhibits synthesis of the first residue of the tetrasaccharide linker[44,45]. Second, genetic ablation of Sox9, a transcription factor, inhibits expression of some CS-synthesizing enzymes (for example, Xylt1/2 and C4st1)[46]. Each strategy is effective in inhibiting CS synthesis and in improving recovery from SCI. However, based on our new findings, inhibition of T1 should be better than either of those strategies because both of those strategies should inhibit HS synthesis, and HS synthesis promotes axon growth.

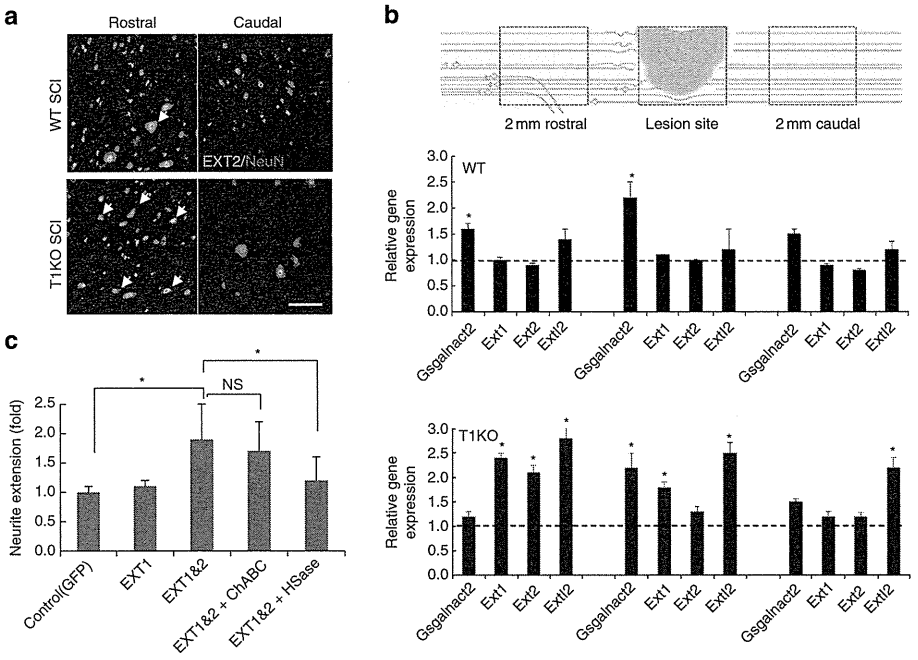

Figure 7 | Elevated expression of HS is necessary to axon regrowth. WT/SCI, WT after SCI; KO/SCI, T1KO after SCI. (**a**) Ext2 (green), an essential enzyme for HS sugar chain synthesis, was upregulated in and localized to neurons of T1KO mice after SCI. NeuN (red), a neuronal marker; Ext2-expressing cells (arrows). Scale bars, 20 μm. (**b**) Reverse transcriptase (RT)-PCR of genes encoding enzymes involved in GAG synthesis after SCI. The samples were collected from three sites in wild-type (WT) or T1KO mice: 2 mm rostral from the lesion centre (left), the lesion centre (centre) and 2 mm caudal from the lesion centre (right). The samples were analysed using RT-PCR. Notably, the rostral site was mainly composed of neurons, not of reactive astrocytes (the left-most cartoon). The average expression of each gene in intact WT or in intact T1KO mice was defined as 1.0. Expression of each gene (*Csgalnact2 (T2), Ext1, Ext2* or *Extl2*) in TIKO versus that in *WT*. $^*P<0.05$ ($n=6$; Bonferroni's comparison test). (**c**) Overexpression of Ext1/Ext2 promoted axon outgrowth of WT cortical neurons in an HSase-dependent manner. Both *Ext1* and *Ext2* complementary DNAs (Ext1 and 2) were transfected into cultured neurons. The Ext1 and Ext2 proteins are thought to form a heterodimeric complex during HS synthesis; overexpression of *Ext1* alone did not result in a significant change. $^*P<0.05$ (one-way ANOVA; $n=4$); *Ext1&2* versus control (*GFP*) or versus *Ext1&2* + HSase. In each individual experiment, 100 neurons were counted and the experiments were performed at least three times. Data are expressed as the mean ± s.e.m. in **b** and **c**.

In conclusion, our results demonstrate that knocking out a single enzyme, T1, caused both reduced CS synthesis and increased HS synthesis and that manipulation of this single enzyme resulted in the reduction of extracellular inhibitors and the induction of intrinsic growth promoters of axon regeneration. Therefore, our findings provide a novel principle for development of axon regeneration strategies. Chemicals that specifically inhibit T1 might be effective treatments for SCI; however, we need to know the molecular mechanisms by which neuronal HS-synthesis genes (for example, *Ext2*) were upregulated in T1KO mice. Finally, adding inhibition of TI to other treatments[36,47] for SCI may improve overall clinical outcomes.

Methods

Materials. ChABC and HSase (HSase I/III), heparanase I and II, WFA and AteloGene Local Use Kits for atelocollagen-mediated *in vivo* short interfering RNA were purchased from Seikagaku Corp. (Tokyo, Japan), from IBEX Technology Inc. (Montreal, Canada), Vector Laboratories Inc. (Burlingame, CA, USA) and from KOKEN Co. Ltd. (Tokyo, Japan), respectively. An osmotic minipump (Model 2006 (for 7W long) and Model 2004 (for 4W long)), catheter tubing (Mit-02) and the infusion kit were purchased from ALZET (Cupertino, CA). Antibodies used in this study are listed in Supplementary Table S1 (As for the two antibodies provided from other researchers, listed in this Table, please refer to refs 48,49).

Generation of T2KO. All animal experimental studies were conducted with the approval of the Animal Care and Use Committee of Niigata University. T1KO[29] mice were derived from the C57BL/6N strain. For most experiments, the WT strain used was C57BL/6N; the ICR strain was used only for the *in vivo* RNAi studies. T2KO mice were generated via the methods used to generate T1KO mice[31]. The mouse *T2* gene was identified as NM_030165. Exon 5 of mouse *T2* encodes a DXD motif, which is a binding site for Mn^{2+} that is essential to the *in vitro* activity of most GalNAc/Gal transferases[50]; therefore, we designed a targeting vector with the mouse *T2* exon 5 located between two loxP sites (Supplementary Fig. S1a). The T2KO mice were generated using an embryonic stem (ES) cell line derived from C57BL/6N mice; this line is designated RENKA. Resulting chimeric mice were mated to C57BL/6N mice and heterozygous offspring (*CSGalNAcT2*$^{+/flox(neo)}$) were mated to *telencephalin-cre* mice[29].

Induction of SCI. Mice (8–10 weeks old, C57BL/6J, male) were subject to compression-induced SCI; a bilateral contusion injury was induced at the 10th thoracic vertebrae (Th10) of individual mice with a commercially available SCI device (Infinite Horizon Impactor; Precision Systems and Instrumentation, Lexington, NY)[20,32], except that here we used a 70-kdyne impact force. The device reports data regarding time versus force and time versus displacement. The locomotor recovery assessment was performed using video recording[32], and BMS open-field scoring was used to test mice once weekly for functional recovery during the 6–8 weeks following SCI[32]. The evaluations were scored independently by two investigators who were unaware of the experimental groups (at least eight mice in each group). On the third day after induction of SCI, mice were excluded if they had an incomplete injury (BMS score > 0 on that day). Morphometric assays were performed using SCI samples prepared from the sagittal sections at 12 μm intervals[32].

For each footfall test, a mouse was placed on a wire mesh grid and videotaped for 5 min while on the grid. To be scored, an animal had to walk for a minimum of 3 of the 5 min as determined by three independent examiners; for each animal scored, the total number of the footfalls from the bars was counted, and the total walking time was recorded.

To assess stepping patterns of hind limbs during forward locomotion after injury, the bottom of a well-lit runway (3 cm wide and 100 cm long) was lined with white paper, and mice were required to run along the runway in a darkened box. To record footprints, the planter surfaces of hind limbs were brushed with ink during continuous locomotion across a paper.

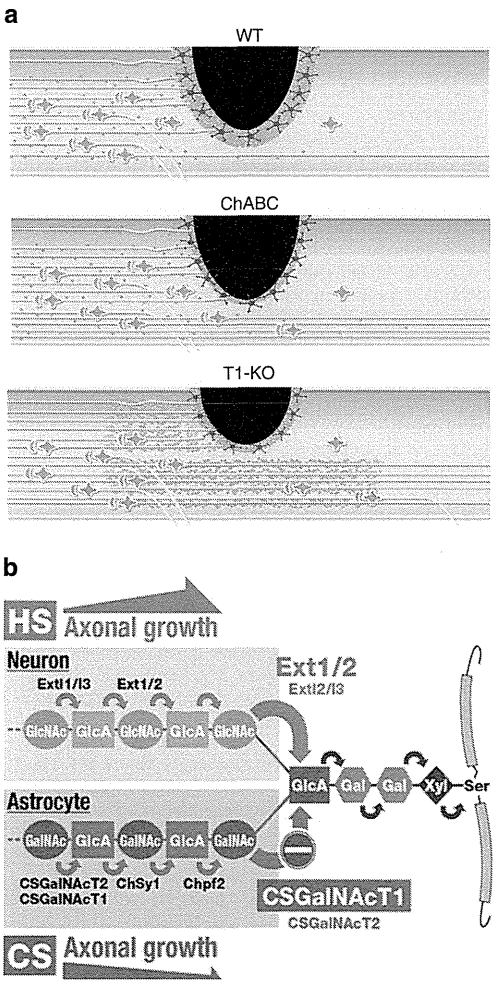

Figure 8 | Schematic model of T1-regulated GAG balance after SCI. (**a**) Summary of the results on SCI recovery. In WT (uppermost) mice, CS (dark pink) production was elevated in the reactive astrocytes (star-like form in blue), and thick scars (black)[3], which inhibited axon regeneration, formed; consequently, very few regenerating axons could migrate to areas past the SCI lesion. In contrast, in T1KO mice (middle), CS production was reduced and the scars were smaller than those in WT mice. In addition, HS (green) expression was high in T1KO neurons, and the number of regrowing or sprouting axons was higher than that in WT. Although ChABC-treated mice (ChABC; lowermost) had less CS than did WT or T1KO, they had larger scars than T1KO mice, and they did not overproduce HS; therefore, axonal regeneration was reduced and restricted relative to that in T1KO. WT and ChABC-treated mice, unlike T1KO mice, experienced only baseline levels of HS synthesis after SCI; these baseline levels could not promote recovery from SCI. (**b**) Possible biochemical mechanism that promotes better recovery from SCI in T1KO mice[26]. In WT, T1 is upregulated in reactive astrocytes after SCI; however, *Ext1* and *Ext2*, which are genes with putative 'axon growth-promoting activity/potential', are upregulated in neurons of T1KO mice, and T1 is not expressed (minus in red); consequently, HS, rather than CS, accumulates around T1KO neurons. As a result, the amount of CS decreases and that of HS increases, and this shift in the CS-HS balance promotes axon regrowth[39]. As increases in HS and decreases in CS persist, the potential for axon growth is elevated.

The electrophysiological experiments to evaluate motor function resulting from evoked potential of the neuromuscular function were performed by short trains of five square-wave stimuli of 0.5 ms duration with an interstimulus interval of 3 ms (ref. 32). The active and the reference electrodes were placed in the muscle belly, and near the distal tendon of the muscle in each limb[32], respectively. Scorps3 software (AD Instruments, New South Wales, Australia) was used to average and analyse 100 responses including the latency period.

Quantitative real-time PCR. Total RNA was extracted from the SCI regions using an RNeasy FFPE kit or an ALL prep RNA kit (QIAGEN). Total RNA (0.5 μg) was used as template; the iScript one-step RT-PCR kit (Bio-Rad), the SsoFast Probes supermix (Bio-Rad) and the PrimeTime qPCR assay (Integrated DNA Technologies, IW) were use for real-time reverse transcriptase–PCR; the reaction parameters were as follows: 95 °C for 30 s; and 40 cycles at 95 °C for 2 s and 65 °C for 5 s; 65–95 °C for 2 s) as indicated in the Taqman probe (Life Technologies) gene expression assay materials. Nucleotide sequence of real-time quantitative PCR primers and ZEN double-quenched probes are listed in Supplementary Table S2.

***In vivo* RNAi after SCI.** For the *in vivo* RNAi studies, SCI was induced in ICR mice (8–10 w; Clea Japan, Inc.) with the IH impactor as described above except that the impact force was 100 kdynes. Just after the SCI contusion, gelfoam impregnated with a mixture containing one or two siRNAs (10 μM each) and AteloGene Local Use Kit (see Materials) was placed on the lesion area[51–53]. RNA sequences of the siRNAs used in these experiments are listed in Supplementary Table S3[54]. The scrambled sequences of the negative-control siRNAs had four or five nucleotides that differed from the corresponding nucleotides in the targeted siRNAs.

ChABC and HSase treatments *in vivo*. Continuous ChABC treatment after SCI was performed using an osmotic pump[14,55] set at the 10th thoracic vertebrae levels for up to 2 weeks (200 U ml^{-1} in a volume of 0.2 ml). For the HSase application, an osmotic minipump (ALZET, Cupertino, CA; Model 2006) was implanted subcutaneously and used to infuse HSase (0.2 unit per 6 μg) dissolved in saline containing 0.05% BSA or vehicle into the contusion site through a flexible plastic cannula because HSase is less stable than ChABC *in vivo*.

Immunohistochemistry. The dilution ratios for each antibody are listed in Supplementary Table S1. Tissue sections were incubated with biotinylated secondary antibody and then with avidin–biotin peroxide complex[55,56] (Vectastain ABC kit; Vector Laboratories Inc.). Digital images were taken with a confocal laser scanning microscope (Zeiss, LSM5 exciter) and AxioVision charge-coupled device camera (Carl Zeiss). Spinal cord cryosections (20 μm thick) were obtained from mice that had been transcardially perfused with 4% formaldehyde. Standardized areas for sampling[32] in the central regions (10 sections) were calculated using Image J (NIH) and MetaMorph (Molecular Devices). For analysis of 5HT(+) sprouting axons and boutons, rectangular areas were set 1–3 mm distal to the central line of the lesion site in each section[32], and 10 sagittal sections from each mouse were used for quantitative analysis.

Anterograde labelling of the CST. Exactly 8 weeks after injury, BDA (10% in saline, molecular weight 10,000 Da; Molecular probes)[6] was injected into the motor cortices to label the descending CST fibres. The injection site was precisely 2.1 mm posterior to the bregma, 2 mm lateral to the bregma and 0.7 mm deep. We performed pressurized injections with a glass capillary attached to a microsyringe (Narishige) at a rate of 0.1 μl min^{-1} until the desired amount was injected. Exactly 2 weeks after each injection, the animals were anaesthetized and perfused with PBS and then with 4% paraformaldehyde in PBS. We used Alexa Fluor 488-conjugated streptavidin (Invitrogen) and the Vectastain ABC Elite kit (Vector Laboratories Inc.) or a tyramide signal amplification fluorescence system (Perkin Elmer) to fluorescently label the BDA.

Quantification analysis of GAGs from the spinal cord. GAG analyses were conducted by enzymatic treatment and HPLC-based quantification[29,57]. GAGs were extracted from spinal cord tissue samples by incubating the samples in a protease solution (0.01 mg actinase E, 10 mM $CaCl_2$, 50 mM Tris–HCl (pH 8.0)) at 55 °C for 2 days. After addition of trichloroacetate, each extract was centrifuged at 15,000 *g* for 20 min. Each partially purified CSPG and HSPG fractions was digested with ChABC (5 mIU ChABC in 60 mM CH_3COONa, 50 mM Tris–HCl (pH 8.0)) or HSase (0.5 mIU HSase in 20 mM CH_3COONa, 2 mM $(CH_3COO)_2Ca$ (pH 7.0)), respectively. GAGs in each digests were derivatized using 2-aminobenzamide; these mixtures were analysed using HPLC (column: YMC pack PA, elution: 16–530 mM NaH_2PO_4)[57].

Neuronal cell culture. Cortical neurons were prepared from embryonic day 17 or postnatal day 1 mice[33], and were then transfected with a human Ext1 construct in a pCMVvector (Takara Bio Co., Otsu, Japan), a human Ext2 construct in the pcDNA3.1 vector (Invitrogen) or a combination thereof. Stealth Select RNAi (Invitrogen, s72517, s72516 and s72518) was used to knockdown RPTPσ expression. In some cultures, ChABC (2 mU) or HSase (2 mU) was added 12 h after transfection. Cells were stained with anti-HS 10E4 antibody 48 h after transfection. The sequences of siRNAs targeting RPTPσ are listed in Supplementary Table S3. siRNAs with scrambled sequence (Invitrogen) were used as negative controls.

Statistics. Data are presented as mean values ± s.e.m. Prism version 5.04 software (GraphPad) or SPSS statistics software (IBM) were used for to perform statistical analyses. Unpaired two-tailed Student's *t*-tests were used for single comparisons. Analysis of variance (ANOVA; one-way, two-way or repeated-measures ANOVA) were used for multiple comparisons; Bonferroni's procedure were used to assess *post hoc* pairwise differences. Repeated-measures ANOVA was used to analyse BMS and footfall scores with follow-up comparison of treatments for each day, by contrast *t*-test and correction for multiple comparisons by the Holm method ($P = 0.05$). Each investigator was blinded with regard to genotypes during all procedures performed to collect data for subsequent statistical analysis. For analyses of the morphometric data, all evaluations were performed by ANOVA with *post hoc*-independent pairwise analysis. $P < 0.05$ was considered statistically significant. The specific tests used to analyse data from each set of experiments are indicated in the figure legends.

References

1. Tuszynski, M. H. & Steward, O. Concepts and methods for the study of axonal regeneration in the CNS. *Neuron* **74,** 777–791 (2012).
2. Esposito, E. & Cuzzocrea, S. Anti-TNF therapy in the injured spinal cord. *Trends Pharmacol. Sci.* **32,** 107–115 (2011).
3. Silver, J. & Miller, J. H. Regeneration beyond the glial scar. *Nat. Rev. Neurosci.* **5,** 146–156 (2004).
4. Liu, K., Tedeschi, A., Park, K. & He, Z. Neuronal intrinsic mechanisms of axon regeneration. *Annu. Rev. Neurosci.* **34,** 131–152 (2011).
5. Bandtlow, C. E. & Zimmermann, D. R. Proteoglycan in the developing brain: new conceptual insights for old proteins. *Physiol. Rev.* **80,** 1267–1290 (2000).
6. Bradbury, E. J. *et al.* Chondroitinase ABC promotes functional recovery after spinal cord injury. *Nature* **416,** 636–640 (2002).
7. Carulli, D., Laabs, T., Geller, H. M. & Fawcett, J. W. Chondroitin sulfate proteoglycans in neural development and regeneration. *Curr. Opin. Neurobiol.* **15,** 116–120 (2005).
8. Lee, J. K. *et al.* Combined genetic attenuation of myelin and Semaphorin-mediated growth inhibition is insufficient to promote serotonergic axon regeneration. *J. Neurosci.* **30,** 10899–10904 (2010).
9. Liu, K. *et al.* PTEN deletion enhances the regenerative ability of adult corticospinal neurons. *Nat. Neurosci.* **13,** 1075–1083 (2010).
10. Yang, P. & Yang, Z. Enhancing intrinsic growth capacity promotes adult CNS regeneration. *J. Neurol. Sci.* **312,** 1–6 (2012).
11. Moore, D. L. *et al.* KLF family members regulate intrinsic axon regeneration ability. *Science* **326,** 298–301 (2009).
12. Jones, L. L., Yamaguchi, Y., Stallcup, W. B. & Tuszynski, M. H. NG2 is a major chondroitin sulfate proteoglycan produced after spinal cord injury and is expressed by macrophages and oligodendrocyte progenitors. *J. Neurosci.* **22,** 2792–2803 (2002).
13. Zhao, R. R. *et al.* Lentiviral vectors express chondroitinase ABC in cortical projections and promote sprouting of injured corticospinal axons. *J. Neurosci. Methods* **201,** 228–238 (2011).
14. Ikegami, T. *et al.* Chondroitinase ABC combined with neural stem/progenitor cell transplantation enhances graft cell migration and outgrowth of growth-associated protein-43-positive fibers after rat spinal cord injury. Eur. *J. Neurosci.* **22,** 3036–3046 (2005).
15. Massey, J. M. *et al.* Increased chondroitin sulfate proteoglycan expression in denervated brainstem targets following spinal cord injury creates a barrier to axonal regeneration overcome by chondroitinase ABC and neurotrophin-3. *Exp. Neurol.* **209,** 426–445 (2008).
16. Starkey, M. L., Bartus, K., Barritt, A. W. & Bradbury, E. J. Chondroitinase ABC promotes compensatory sprouting of the intact corticospinal tract and recovery of forelimb function following unilateral pyramidotomy in adult mice. *Eur. J. Neurosci.* **36,** 3665–3678 (2012).
17. Bradbury, E. J. & Carter, L. M. Manipulating the glial scar: chondroitinase ABC as a therapy for spinal cord injury. *Brain Res. Bull.* **84,** 306–316 (2011).
18. Zhao, R. R. & Fawcett, J. W. Combination treatment with chondroitinase ABC in spinal cord injury-breaking the barrier. *Neurosci. Bull.* **29,** 477–483 (2013).
19. Rolls, A., Shechter, R. & Schwartz, M. The bright side of the glial scar in CNS repair. *Nat. Rev. Neurosci.* **10,** 235–241 (2009).
20. Okada, S. *et al.* Conditional ablation of Stat3 or Socs3 discloses a dual role for reactive astrocytes after spinal cord injury. *Nat. Med.* **12,** 829–834 (2006).
21. Sato, T. *et al.* Differential roles of two *N*-acetylgalactosaminyltransferases, CSGalNAcT-1, and a novel enzyme, CSGalNAcT-2: Initiation and elongation in synthesis of chondroitin sulfate. *J. Biol. Chem.* **278,** 3063–3071 (2003).
22. Uyama, T., Kitagawa, H., Tamura, J. & Sugahara, K. Molecular cloning and expression of human chondroitin N-acetylgalactosaminyltransferase: the key enzyme for chain initiation and elongation of chondroitin/dermatan sulfate on the protein linkage region tetrasaccharide shared by heparin/heparan sulfate. *J. Biol. Chem.* **277,** 8841–8846 (2002).
23. Mizumoto, S., Ikegawa, S. & Sugahara, K. Human genetic disorders caused by mutations in genes encoding biosynthetic enzymes for sulfated glycosaminoglycans. *J. Biol. Chem.* **288,** 10953–10961 (2013).
24. Nadanaka, S. & Kitagawa, H. Heparan sulphate biosynthesis and disease. *J. Biochem.* **144,** 7–14 (2008).
25. Maeda, N., Ishii, M., Nishimura, K. & Kamimura, K. Functions of chondroitin sulfate and heparan sulfate in the developing brain. *Neurochem. Res.* **36,** 1228–1240 (2011).
26. Duchez, S. *et al.* Glycotranscriptome study reveals an enzymatic switch modulating glycosaminoglycan synthesis during B-cell development and activation. *Eur. J. Immunol.* **41,** 3632–3644 (2011).
27. Uyama, T. *et al.* Molecular cloning and expression of a second chondroitin *N*-acetylgalactosaminyltransferase involved in the initiation and elongation of chondroitin/dermatan sulfate. *J. Biol. Chem.* **278,** 3072–3078 (2003).
28. Gulberti, S. *et al.* Chondroitin sulfate *N*-acetylgalactosaminyltransferase-1 (CSGalNAcT-1) involved in chondroitin sulfate initiation: Impact of sulfation on activity and specificity. *Glycobiology* **22,** 561–571 (2012).
29. Watanabe, Y. *et al.* Chondroitin sulfate *N*-acetylgalactosaminyltransferase-1 is required for normal cartilage development. *Biochem. J.* **432,** 47–55 (2010).
30. Murakami, K. *et al.* Nerve injury induces the expression of EXT2, a glycosyltransferase required for heparan sulfate synthesis. *Neuroscience* **141,** 1961–1969 (2006).
31. Kantor, D. B. *et al.* Semaphorin 5A is a bifunctional axon guidance cue regulated by heparan and chondroitin sulfate proteoglycans. *Neuron* **44,** 961–975 (2004).
32. Ito, Z. *et al. N*-Acetylglucosamine 6-*O*-sulfotransferase-1-deficient mice show better functional recovery after spinal cord injury. *J. Neurosci.* **30,** 5937–5947 (2010).
33. Nozumi, M. *et al.* Identification of functional marker proteins in the mammalian growth cone. *Proc. Natl Acad. Sci. USA* **106,** 17211–17216 (2009).
34. Izumikawa, T. *et al.* Nematode chondroitin polymerizing factor showing cell-/organ-specific expression is indispensable for chondroitin synthesis and embryonic cell division. *J. Biol. Chem.* **279,** 53755–53761 (2004).
35. Wang, D. & Fawcett, J. The perineuronal net and the control of CNS plasticity. *Cell Tissue Res.* **349,** 147–160 (2012).
36. Alilain, W. J., Horn, K. P., Hu, H., Dick, T. E. & Silver, J. Functional regeneration of respiratory pathways after spinal cord injury. *Nature* **475,** 196–200 (2011).
37. Massey, J. M. *et al.* Chondroitinase ABC digestion of the perineuronal net promotes functional collateral sprouting in the cuneate nucleus after cervical spinal cord injury. *J. Neurosci.* **26,** 4406–4414 (2006).
38. Shen, Y. *et al.* PTPσ is a receptor for chondroitin sulfate proteoglycan, an inhibitor of neural regeneration. *Science* **326,** 592–595 (2009).
39. Coles, C. H. *et al.* Proteoglycan-specific molecular switch for RPTPσ clustering and neuronal extension. *Science* **332,** 484–488 (2011).
40. Bloechlinger, S., Karchewski, L. A. & Woolf, C. J. Dynamic changes in glypican-1 expression in dorsal root ganglion neurons after peripheral and central axonal injury. *Eur. J. Neurosci.* **19,** 1119–1132 (2004).
41. Hsueh, Y. P. & Sheng, M. Regulated expression and subcellular localization of syndecan heparan sulfate proteoglycans and the syndecan-binding protein CASK/LIN-2 during rat brain development. *J. Neurosci.* **19,** 7415–7425 (1999).
42. Matsuo, I. & Kimura-Yoshida, C. Extracellular modulation of Fibroblast growth factor signaling through heparan sulfate proteoglycans in mammalian development. *Curr. Opin. Genet. Dev.* **23,** 399–407 (2013).
43. Inatani, M. & Yamaguchi, Y. Gene expression of EXT1 and EXT2 during mouse brain development. *Brain Res. Dev. Brain Res.* **141,** 129–136 (2003).
44. Grimpe, B. & Silver, J. A novel DNA enzyme reduces glycosaminoglycan chains in the glial scar and allows microtransplanted dorsal root ganglia axons to regenerate beyond lesions in the spinal cord. *J. Neurosci.* **24,** 1393–1397 (2004).
45. Oudega, M. *et al.* Systemic administration of a deoxyribozyme to xylosyltransferase-1 mRNA promotes recovery after a spinal cord contusion injury. *Exp. Neurol.* **237,** 170–179 (2012).
46. McKillop, W. M., Dragan, M., Schedl, A. & Brown, A. Conditional Sox9 ablation reduces chondroitin sulfate proteoglycan levels and improves motor function following spinal cord injury. *Glia* **61,** 164–177 (2013).
47. Tsuji, O. *et al.* Therapeutic potential of appropriately evaluated safe-induced pluripotent stem cells for spinal cord injury. *Proc. Natl Acad. Sci. USA* **107,** 12704–12709 (2010).
48. Uetani, N. *et al.* Mammalian motoneuron axon targeting requires receptor protein tyrosine phosphatases sigma and delta. *J. Neurosci.* **26,** 5872–5880 (2006).
49. Kobayashi, S. *et al.* Association of EXT1 and EXT2, hereditary multiple exostoses gene products, in Golgi apparatus. *Biochem. Biophys. Res. Commun.* **268,** 860–867 (2000).
50. Lairson, L. L., Henrissat, B., Davies, G. J. & Withers, S. G. Glycosyltransferases: structures, functions, and mechanisms. *Annu. Rev. Biochem.* **77,** 521–555 (2008).
51. Mu, P. *et al.* Systemic delivery of siRNA specific to tumor mediated by atelocollagen: combined therapy using siRNA targeting Bcl-xL and cisplatin against prostate cancer. *Int. J. Cancer* **125,** 2978–2990 (2009).
52. Wang, X. *et al.* Ibuprofen enhances recovery from spinal cord injury by limiting tissue loss and stimulating axonal growth. *J. Neurotrauma* **26,** 81–95 (2009).

53. Boato, F. *et al.* C3 peptide enhances recovery from spinal cord injury by improved regenerative growth of descending fiber tracts. *J. Cell Sci.* **123,** 1652–1662 (2010).
54. Lin, R., Kwok, J. C. F., Crespo, D. & Fawcett, J. W. Chondroitinase ABC has a long-lasting effect on chondroitin sulfate glycosaminoglycan content in the injured rat brain. *J. Neurochem.* **104,** 400–408 (2008).
55. Li, H. P. *et al.* Regeneration of nigrostriatal dopaminergic axons by degradation of chondroitin sulfate is accompanied by elimination of the fibrotic scar and glia limitans in the lesion site. *J. Neurosci. Res.* **85,** 536–547 (2007).
56. Yoshioka, N. *et al.* Small molecule inhibitor of type I transforming growth factor-β receptor kinase ameliorates the inhibitory milieu in injured brain and promotes regeneration of nigrostriatal dopaminergic axons. *J. Neurosci. Res.* **89,** 381–393 (2011).
57. Kitagawa, H., Kinoshita, A. & Sugahara, K. Microanalysis of glycosaminoglycan-derived disaccharides labeled with the fluorophore 2-aminoacridone by capillary electrophoresis and high-performance liquid chromatography. *Anal. Biochem.* **232,** 114–121 (1995).

Acknowledgements

We thank M. Nakamura, T. Yamashita, M. Abematsu and K. Nakashima for instruction and advice on the SCI experiments; T. Shirasawa and M.L. Tremblay for antibodies; and I. Hasegawa and Y. Tada-Kinoshita for technical assistance. Generation of the T1KO and T2KO mice was supported by the TOGONO support group from the MEXT of Japan, and some antibodies were produced by Everest Biotech Ltd. (Upper Heyford, UK) for its Antibody award. This work was supported in part by KAKENHI (#17023019, #22022040 and #24111515 to M.I., #23592161 and #24110503 to K.T. and #23700440 to S.H.O.), Project Promoting Grants from Niigata University to M.I. and Agri-Health Translational Research Project support (#4300) from Ministry of the Agriculture, Forestry and Fisheries of Japan to K.T. Post-doctoral grants from JSPS supported N.Y. and Y.W.

Author contributions

M.I. and K.T. designed the experiments, and analysed the data. Y. Watanabe, K.Oh, K.Od, T.S., M.Y. and K.S. produced the gene-targeted mice. N.Y., S.H.O., M.O., C.K., Y. Wada and H. Kawano developed the SCI model and performed the biochemical and the histological experiments. N.M. designed the siRNA sequences. M.N. and H.O. taught members of the lab the techniques necessary for the SCI model. S.M. and H. Kitagawa performed the quantitative analysis of CS and HS. M.I. wrote the paper, and in part, K.T. wrote the Methods section.

Additional information

Supplementary Information accompanies this paper at http://www.nature.com/naturecommunications

Competing financial interests: The authors declare no competing financial interests.

Reprints and permission information is available online at http://npg.nature.com/reprintsandpermissions/

How to cite this article: Takeuchi, K. *et al.* Chondroitin sulphate *N*-acetylgalactosaminyl-transferase-1 inhibits recovery from neural injury. *Nat. Commun.* 4:2740 doi:10.1038/ncomms3740 (2013).

Neuron
Report

Increased L1 Retrotransposition in the Neuronal Genome in Schizophrenia

Miki Bundo,[1,2] Manabu Toyoshima,[3] Yohei Okada,[4] Wado Akamatsu,[4] Junko Ueda,[2] Taeko Nemoto-Miyauchi,[2] Fumiko Sunaga,[1] Michihiro Toritsuka,[5] Daisuke Ikawa,[5] Akiyoshi Kakita,[6] Motoichiro Kato,[7] Kiyoto Kasai,[8] Toshifumi Kishimoto,[5] Hiroyuki Nawa,[9] Hideyuki Okano,[4] Takeo Yoshikawa,[3] Tadafumi Kato,[2,*] and Kazuya Iwamoto[1,10,*]
[1]Department of Molecular Psychiatry, Graduate School of Medicine, The University of Tokyo, Tokyo 113-8655, Japan
[2]Laboratory for Molecular Dynamics of Mental Disorders
[3]Laboratory for Molecular Psychiatry
RIKEN Brain Science Institute, Saitama 351-0198, Japan
[4]Department of Physiology, Keio University School of Medicine, Tokyo 160-8582, Japan
[5]Department of Psychiatry, Nara Medical University, Nara 634-8521, Japan
[6]Department of Pathology, Brain Research Institute, Niigata University, Niigata 951-8585, Japan
[7]Department of Neuropsychiatry, Keio University School of Medicine, Tokyo 160-8582, Japan
[8]Department of Neuropsychiatry, Graduate School of Medicine, The University of Tokyo, Tokyo 113-8655, Japan
[9]Department of Molecular Neurobiology, Brain Research Institute, Niigata University, Niigata 951-8585, Japan
[10]PRESTO, Japan Science and Technology Agency, Saitama 332-0012, Japan
*Correspondence: kato@brain.riken.jp (T.K.), kaziwamoto-tky@umin.ac.jp (K.I.)
http://dx.doi.org/10.1016/j.neuron.2013.10.053

SUMMARY

Recent studies indicate that long interspersed nuclear element-1 (L1) are mobilized in the genome of human neural progenitor cells and enhanced in Rett syndrome and ataxia telangiectasia. However, whether aberrant L1 retrotransposition occurs in mental disorders is unknown. Here, we report high L1 copy number in schizophrenia. Increased L1 was demonstrated in neurons from prefrontal cortex of patients and in induced pluripotent stem (iPS) cell-derived neurons containing 22q11 deletions. Whole-genome sequencing revealed brain-specific L1 insertion in patients localized preferentially to synapse- and schizophrenia-related genes. To study the mechanism of L1 transposition, we examined perinatal environmental risk factors for schizophrenia in animal models and observed an increased L1 copy number after immune activation by poly-I:C or epidermal growth factor. These findings suggest that hyperactive retrotransposition of L1 in neurons triggered by environmental and/or genetic risk factors may contribute to the susceptibility and pathophysiology of schizophrenia.

INTRODUCTION

Mental disorders including schizophrenia, bipolar disorder, and major depression affect a large proportion of the global population and have a major negative economic impact. Twin, family, and adoption studies indicate the complex involvement of both genetic and environmental factors for these diseases (Keshavan et al., 2011). Despite their apparent heritability, however, causative genetic factors are mostly unknown except for rare cases of schizophrenia associated with chromosomal abnormalities (Brandon and Sawa, 2011; Cook and Scherer, 2008; Karayiorgou et al., 2010). On the other hand, environmental risk factors including prenatal infection (Brown, 2006) and obstetric complications, such as neonatal hypoxia, embryonic ischemia, and gestational toxicosis (Lewis and Murray, 1987), are well-established risk factors for schizophrenia. However, it is not clarified how these environmental risk factors interact with genomic factors.

Accumulating evidence indicates that genomic DNA in the brain contains distinctive somatic genetic variations compared with nonbrain tissues (Poduri et al., 2013). These genetic signatures include brain-specific somatic mutations (Poduri et al., 2013), chromosomal aneuploidy (Rehen et al., 2005; Yurov et al., 2007), chromosomal microdeletion (Shibata et al., 2012), and the genome dynamics of nonlong terminal repeat (LTR) retrotransposons (Baillie et al., 2011; Evrony et al., 2012; Muotri and Gage, 2006). These observed somatic variations are hypothesized to contribute to the generation of functionally diversified brain cells (Muotri and Gage, 2006).

Among the known retrotransposons, only long interspersed nucleotide element-1 (L1) has autonomous retrotransposition activity. Full-length L1 elements include a 5′ UTR, two open reading frames (ORFs), and a 3′ UTR (Figure 1A). Encoded products from the ORFs contain activities required for retrotransposition and are employed in the insertion of new L1 copies as well as nonautonomous retrotransposons such as *Alu* and SVA (Cordaux and Batzer, 2009). Recent studies indicate that engineered L1 has retrotransposition activity in neural progenitor cells from rat hippocampus (Muotri et al., 2005), human fetal brain (Coufal et al., 2009), and human embryonic stem cells (Coufal et al., 2009). These in vitro findings were confirmed in human L1 transgenic mice in vivo (Muotri et al., 2005). Adult human brain cells also showed increased L1 copy number compared with nonbrain tissues (Coufal et al., 2009). Moreover, retrotransposition

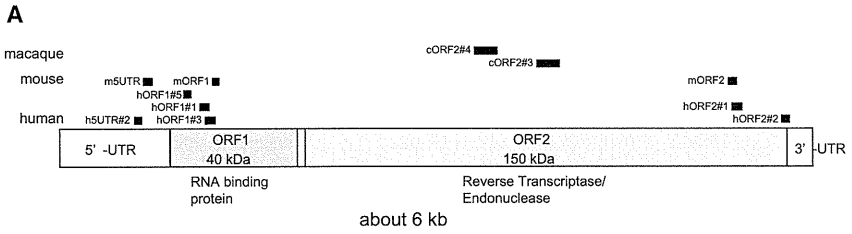

B

set	diagnosis	n	gender (F:M)	age	onset (yrs)	suicide	side (R:L)	pH	PMI (hrs)
I	CT	13	5:8	48.2±10.4	-	0	5:8	6.2±0.2	23.6±10.7
I	SZ	13	5:8	44.4±12.9	24.2±8.1	3	6:7	6.2±0.3	34.7±14.6
I	MD	12	5:7	45.2±10.0	33.5±11.8	6	3:9	6.1±0.2	27.8±10.5
I	BD	13	5:8	41.5±11.2	21.9±8.9	7	7:6	6.1±0.2	31.2±15.2
II	CT	34	8:26	44.5±7.5	-	0	18:16	6.6±0.3	29.5±13.0
II	SZ	35	9:26	42.6±8.5	21.3±6.1	7	18:17	6.5±0.2	31.4±15.3

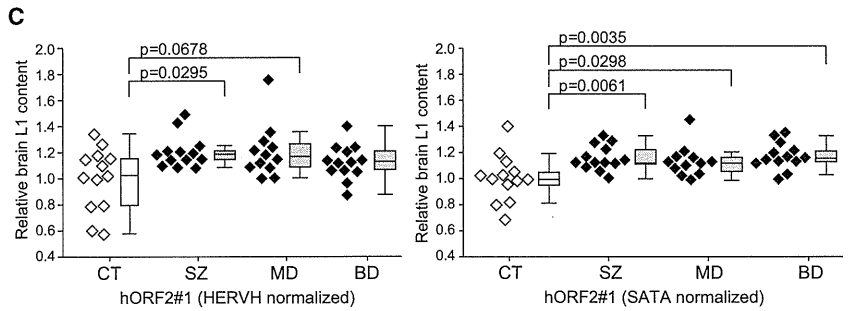

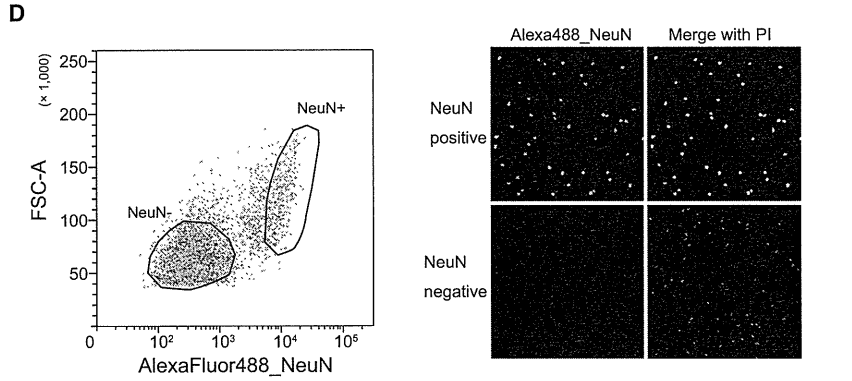

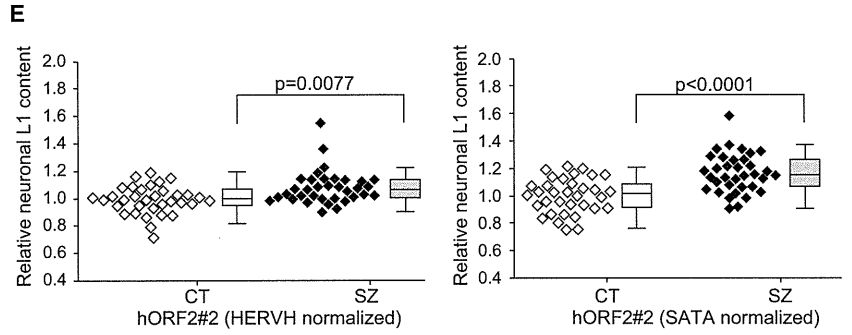

Figure 1. Increase of Brain L1 Copy Number in Schizophrenia

(A) Structure of L1 and map of the primers. Primers and probes are from previous studies (Coufal et al., 2009; Muotri et al., 2010) or designed for this study (Table S4). (B) Summary of the demographic variables of brain samples. (C) L1 copy number in set I. (D) Neuronal nuclei isolation. Left: example of NeuN-based nuclei sorting of brain cells from a patient with schizophrenia. Right: microscopic confirmation of isolated nuclei. The purity of each fraction was >95% and 99.9% for NeuN+ and NeuN−, respectively. (E) Neuronal L1 copy number in set II. In quantitative real-time PCR, L1 copy number was measured with HERVH or SATA as internal controls. The ratio of prefrontal cortex to liver (for set I) or neurons to nonneurons (for set II) was calculated and then normalized relative to the average value of control samples. Values were represented as open or closed diamonds as well as box plots. The ΔCt values of L1 and control probes were not significantly different between diagnostic groups in set I or set II. p values were determined by the Mann-Whitney U test. PMI, postmortem interval; CT, controls; SZ, schizophrenia; MD, major depression; BD, bipolar disorder; PI, propidium iodide. See also Tables S1 and S4 and Figures S1 and S2.

is active in MeCP2 mouse models and patients with Rett syndrome, indicating a role for this mechanism in this Mendelian disorder (Muotri et al., 2010). Together, these findings suggest the hypothesis that L1 retrotransposition may also be involved in the pathophysiology of mental disorders.

In this study, we quantified L1 copy number in genomic DNA derived from postmortem brains of patients with major mental disorders. We report significant increases of L1 content in the prefrontal cortex of patients with schizophrenia. To confirm this finding, we quantified L1 copy number in neurons and nonneurons from a second, independent patient cohort using NeuN-based cell sorting (Iwamoto et al., 2011; Rehen et al., 2005; Spalding et al., 2005) and found that L1 copy number in neurons was increased in patients with schizophrenia. We next quantified L1 copy number in the animal models that are known to disturb early neural development. These included maternal polyriboinosinic-polyribocytidilic acid (poly-I:C) injection in mice (Meyer and Feldon, 2012; Giovanoli et al., 2013) and chronic epidermal growth factor (EGF) injection to infant macaques (Nawa et al., 2000). We found that genomic DNA of brains from both animal models showed increased L1 copy number, addressing the importance of environmental factors during perinatal and postnatal stages. We also found that the increased L1 copy number

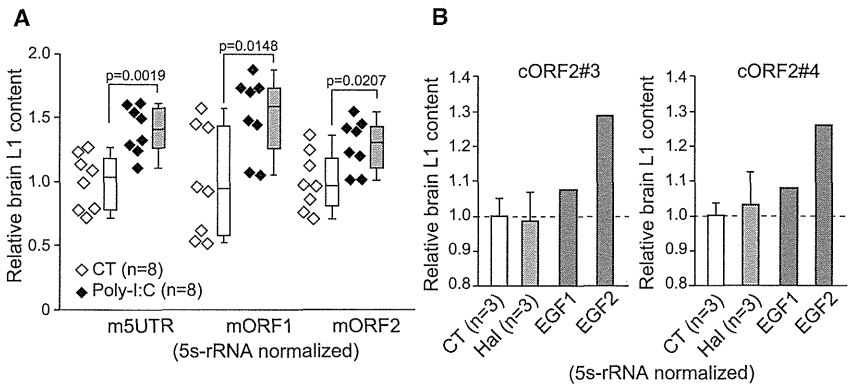

Figure 2. Increase of Brain L1 Copy Number in Animal Models

(A) Brain L1 content in the maternal poly-I:C model. p values were determined by the Mann-Whitney U test. Values were represented as open or closed diamonds as well as box plots. (B) Brain L1 content in chronic EGF or haloperidol-treated macaque models. Error bars indicate SDs. The comparative Ct method, with 5S-rRNA as an internal control, was used. The ratio of prefrontal cortex to liver (for poly-I:C model) or prefrontal gray matter to NeuN-sorted nonneurons in white matter (for macaque models) was calculated and then normalized relative to the average value of control samples. See also Table S4.

in the neurons derived from induced pluripotent stem (iPS) cells of schizophrenia patients with 22q11 deletion. The 22q11 deletion is a well-defined genetic factor and is one of the highest risk factors for schizophrenia, affecting about 1%–2% of schizophrenia patients (Karayiorgou et al., 2010). Finally, we performed whole-genome sequencing (WGS) analysis of brain and liver in controls and patients. Comparison of brain-specific L1 insertion sites revealed that brain-specific L1 insertion in patients is enriched in or near genes related to synaptic function and neuropsychiatric diseases. These results suggest that increased retrotransposition of L1 in neurons, which was triggered by genetic component and/or environmental factors at the early neural development, could contribute to the susceptibility and pathophysiology of schizophrenia.

RESULTS

Increased Brain L1 Content in Schizophrenia

We used postmortem prefrontal cortex samples of patients with schizophrenia, bipolar disorder, and major depression as well as control subjects for analysis in set I. The demographic variables are summarized in Figure 1B. We quantified L1 copy number of postmortem prefrontal cortex and liver in each subject by quantitative RT-PCR with two different internal controls, which were designed for human endogenous retrovirus (HERVH) and alpha-satellite (SATA). We found a significant increase in the brain L1ORF2 content in patients with schizophrenia (Figure 1C). A tendency toward copy number increase was also observed in mood disorders and in other L1 probes in schizophrenia (Figure S1 available online).

Somatic L1 retrotransposition was primarily found in neuronal cells (Kuwabara et al., 2009). To confirm the increased brain L1 copy number in schizophrenia and address whether this copy number increase is due to alteration of the neuronal genome, we examined an independent prefrontal cortex sample set (set II). We separated neuronal and nonneuronal nuclei from frozen brains using NeuN-based cell sorting (Figure 1D) (Iwamoto et al., 2011). NeuN is expressed in vertebrate neurons, and its antibody can be used for labeling neuronal nuclei (Mullen et al., 1992). We quantified L1ORF2 copy number of genomic DNA derived from neurons (NeuN-positive nuclei) and nonneurons (NeuN-negative nuclei) and then calculated the neuron-to-nonneuron ratio. We found a significant increase of neuronal L1ORF2 content in schizophrenia in two different internal controls (Figure 1E). The copy number of the other L1 probes tested also showed significant increase in schizophrenia compared to controls in SATA-normalized data, and similar tendency toward copy number increase was observed in HERVH-normalized data (Figure S1 and data not shown).

Assessment of Confounding Factors

We assessed the effect of confounding factors on L1 content (Table S1). Among the demographic variables tested, sample pH showed a weak correlation with L1ORF2 content in set II but not in set I. Several variables also showed weak correlations, but none showed consistency across the different internal control probes or across the two different sample sets.

To consider the possible effect of antipsychotics, we examined L1 copy number in a human neuroblastoma cell line cultured with haloperidol or risperidone for 8 days. Both antipsychotics did not modify the L1 copy number at their low or high concentrations (Figure S2). Together with the fact that the lifetime intake of antipsychotics, which was estimated as fluphenazine milligram equivalents, did not correlate with L1 copy number in both brain sets (Table S1), medication status did not affect our results.

L1 Quantification in Animal Models

To assess the potential roles of environmental factors on increased L1 copy number, we employed two different animal models that mimic environmental risk factors that affect early neural development. They included maternal poly-I:C injection in mice and chronic EGF injection to neonatal macaques. The poly-I:C, which mimics viral double-stranded RNA, injection to pregnant mice induces elevated maternal immune activation, and the offspring is known to show schizophrenia-like behavioral alterations such as impairments of prepulse inhibition and social behavior at the later stage (Meyer and Feldon, 2012). Pregnant mice received a single intraperitoneal injection of poly-I:C. L1 copy number in the prefrontal cortex of offspring was tested at postnatal day 21. We found that significant elevation of L1 copy number at all the tested probes compared to controls (Figure 2A).

We then examined the L1 copy number in macaques treated with EGF during neonatal period. Perinatal and postnatal

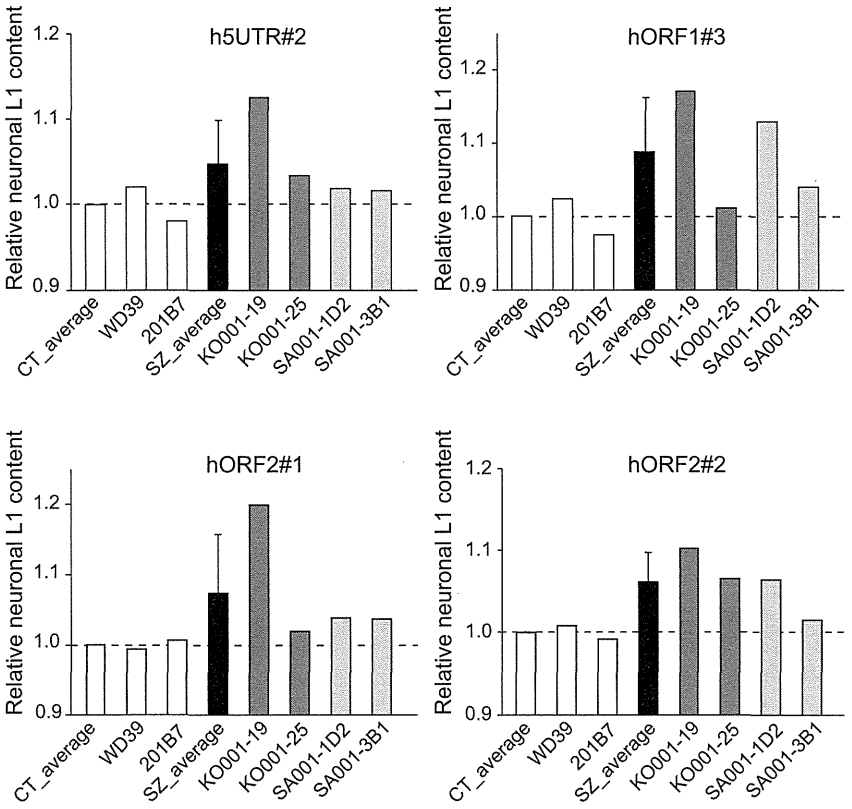

Figure 3. L1 Content in Neurons Derived from iPS Cells of Schizophrenia Patients with 22q11 Deletions
The comparative Ct method, with SATA as an internal control, was used. The ratio of NeuN-sorted neurons to nonneurons was calculated and then normalized relative to average value of control samples. Error bars indicate SDs. See also Table S4 and Figure S3.

perturbation of EGF is known to evoke schizophrenia-like phenotypes, including deficits in prepulse inhibition, latent inhibition, social interaction, and working memory, in adulthood (Nawa et al., 2009, 2000).The neonatal macaques (n = 2) subcutaneously received EGF for seven times over 11 days. After 4 and 7 years from treatment, L1 copy number in the prefrontal cortex was tested. In addition, chronic haloperidol-treated macaques (n = 3) were also tested. Due to unavailability of other tissues, we isolated nonneuronal nuclei from frozen white matter and calculated the grey matter-to-nonneuron ratio in each subject. Although statistical approach could not be applied, we observed increase of L1 copy number in EGF-treated macaques, but not in the haloperidol-treated macaques, compared to controls (Figure 2B). Taken together, these results suggest that early environmental factors play important roles in the L1 content in the brain. We further confirmed that chronic haloperidol treatment did not influence L1 copy number in this model.

L1 Quantification in the iPS Cells of Schizophrenia Patients with 22q11 Deletion

We next assessed the importance of genetic risk factor on the L1 copy number in brain. We quantified L1 copy number in the neurons derived from iPS cells of schizophrenia patients with 22q11 deletion (n = 2) as well as controls (n = 2) (Figure S3). The iPS cells were established from the fibroblasts according to the previously developed method (Imaizumi et al., 2012; Takahashi et al., 2007; M.T., unpublished data). To estimate the L1 copy number, we used two independently established iPS cell lines per patient. After induction of neuronal cells (Imaizumi et al., 2012), we isolated neuronal nuclei by NeuN-based sorting (Figure S3). We then examined L1 copy number and calculated the neuron-to-nonneuron ratio. Compared to controls, we observed consistent increase of L1 copy number in iPS cell-derived neurons of patients with schizophrenia with 22q11 deletion (Figure 3). These results suggest that the well-defined strong genetic risk factor also plays an important role in the L1 content in the brain.

Identification and Comparison of Brain-Specific L1 Transposition

We next performed WGS of brain and liver DNA from same subjects by self-assembling DNA nanoarray technology (Drmanac et al., 2010). For this experiment, schizophrenia patients (n = 3) and control subjects (n = 3) were selected to match age, PMI, gender, brain pH, and race from set I. Selected patients exhibited increased L1 content by quantitative RT-PCR assay, compared to average L1 content of the controls and selected control subjects. The WGS metrics and identified variations were summarized in Table S2. Distribution of the detected mobile elements was almost equal between the tissues and across subjects, and over the half of the identified elements was related